UNIVERSITY OF CALIFORNIA
RIVERSIDE

Trend and Trend Reversal Analysis of Ambient NO_2 Concentration in Europe

A Thesis submitted in partial satisfaction
of the requirements for the degree of

Master of Science

in

Environmental Sciences

by

Yuhua Situ

September 2021

Thesis Committee:
Dr. King-Fai Li, Chairperson
Dr. Roya Bahreini
Dr. William Porter

The Thesis of Yuhua Situ is approved:

Committee Chairperson

University of California, Riverside

Acknowledgements

I would like to thank my advisor, Professor King-Fai Li, for the insightful guidance when I navigated through different areas of research.

Dedication

I dedicate my thesis to my wonderful family. Your support and encouragement are priceless.

ABSTRACT OF THE THESIS

Trend and Trend Reversal Analysis of Ambient NO_2 Concentration in Europe

by

Yuhua Situ

Master of Science, Graduate Program in Environmental Sciences
University of California, Riverside, September 2021
Dr. King-Fai Li, Chairperson

A recent study based on a compiled dataset of satellite NO_2 retrievals covering ~21 years revealed changes in the NO_2 trends, both from positive to negative and vice versa, over some European and Asian regions, contradicting the expected monotonic decreasing trend. In this study, we analyzed the trends in the surface level NO_2 over the European Environment Agency (EEA) member countries. Some studies used station data up to 2013 while some only after 2013. In this study, we compiled a monthly-averaged hourly surface NO_2 dataset that covers the whole period of observation, including before and after 2013. As a result, data availability in some cities extended to about 40 years. To compare the station surface NO_2 with the satellite NO_2 column retrievals, we converted the surface NO_2 into tropospheric NO_2 column by matching the surface NO_2 with that of the NO_2 profile assimilated in the European Centre for Medium-Range Weather Forecasts (ECMWF). 18 European cities were later selected where the converted NO_2 column agreed well with the satellite NO_2 column. We also converted the satellite NO_2 column to surface NO_2 using

the ECMWF profile, but our selection remained unchanged. The long-term trend, changes in diurnal and seasonal cycles, and trend reversals of the selected cities were studied. The selected cities all showed a decreasing trend, and most of the cities already comply with the annual NO_2 limit by EEA. All the cities showed similar diurnal and seasonal cycles, but the morning peaks of NO_2 over some cities have shifted 1–2 hours towards noon, which may imply a shorter NO_2 lifetime over those cities. Trend reversals were detected in most of the cities. However, the time of the reversals detected in ground station data could be quite different from those in the satellite time series, the latter mostly in the early 2000s. The trend reversal points seem to be a part of decadal variability, whose cause needs further investigation. Given the limitation in the trend reversal detection algorithm over finite time series, the reversal points detected in the previous study using short NO_2 records may subject to large uncertainties.

Table of Contents

List of Figures

1 Introduction

1.1. Research Background

Nitrogen dioxide (NO_2) is a member of the NO_x ($NO+NO_2$) family and is one of the primary pollutants in car exhausts (Haagen-Smit, 1950, 1952). Besides thermal NO_x formed by thermolyzed air during high-temperature combustion, combustion of fuels that are rich in nitrogen (e.g., biomass, coal) also contributes to NO_x emission. It was estimated that about 22 Tg N in the form of NO_x was released global in the year of 1980; about 0.85 Tg N per year was released by civil and military aviation in 1992 (Dignon, 1992; Gardner et al., 1997). The presence of NO_x may cause acute respiratory irritation and lead to tropospheric ozone formation, which is yet another lung irritant (Jacob, 2019; Mauzerall et al., 2005). In the meanwhile, ozone's absorption of infrared (IR) radiation causes the troposphere to warm up. In the US, the Environmental Protection Agency (EPA) sets a National Ambient Air Quality Standard (NAAQS) (U.S. EPA, 2016), regulating the hourly NO_2 level below 100 ppb.

As a result of emission reduction efforts in last few decades, significant decrease in global NO_2 concentration has been observed from ground-based and satellite NO_2 observations (van der A. et al., 2008; Georgoulias et al., 2019; Kim et al., 2006, 2009; Konovalov et al., 2010; McDonald et al., 2012; Russell et al., 2010; Stavrakou et al., 2008; Xing et al., 2013). Such efforts include: (1) Reducing combustion temperature to reduce the formation of NO_x during combustion, which is achieved by injecting cooled flue gas, injecting water/steam or using fuel rich or fuel lean mixture to avoid the stoichiometric

ratio; (2) Reducing residence time within internal combustion engines to prevent excess ionization of nitrogen; (3) Reducing NO_x chemically to N_2, using ammonia, urea or unburned hydrocarbons as the reducing agents; (4) Oxidizing NO_x, using ozone, H_2O_2 or a catalyst, in order to raise nitrogen to a higher valence to enhance its solubility in water; and (5) Removing nitrogen from combustion, which can be achieved by using oxygen instead of air in the combustion, or using fuel low in nitrogen content.

Several space-borne instruments, including Global Ozone Monitoring Experiment (GOME) and GOME-2, SCanning Imaging Absorption SpectroMeter for Atmospheric CHartographY (SCIAMACHY), and Ozone Monitoring Instrument (OMI), have been providing global NO_2 measurements, in the form of Vertical Column Density (VCD). These data can be combined to provide a near-continuous NO_2 record since 1995 (Behrens et al., 2018; Geddes et al., 2016; Georgoulias et al., 2019).

Among the space-borne instruments mentioned above, GOME was the first to measure NO_2 VCD. It was launched onboard the second European Remote Sensing satellite (ERS-2) in 1995 by European Space Agency (ESA) and served until September 2011. GOME was an across-track nadir-viewing spectrometer, flying on a solar-synchronous, polar (inclination 98.5 degrees) orbit with a repeat cycle of 35 days and an equator crossing time of 10:30 local time (https://earth.esa.int/documents/10174/1596664/GOME05.pdf). With the largest footprint, the nominal spatial resolution is 320km across-track and 40km along-track. In this mode, GOME could provide global coverage at the equator every 3 days. In June 2003, when the ERS-2 tape recorder became permanently unavailable due to

a technical failure and the coverage was greatly reduced (https://earth.esa.int/sppa-reports/ers-2/gome/reports/yearly/anomalies_2003.html).

Launched by ESA in March 2002, ENVISAT flew an orbit similar to ERS-2 with an equatorial crossing time at 10:00 (https://earth.esa.int/web/guest/missions/esa-operational-eo-missions/envisat/instruments/sciamachy-handbook/wiki). SCIAMACHY onboard ENVISAT provided data from August 2002 to April 2012. With a spatial resolution of 60 km × 30 km, SCIAMACHY provided more detailed observations of polluted areas, such as cities and large power plants (Kim et al., 2006; Richter et al., 2004).

As a successor of GOME and SCIAMACHY, two identical GOME-2 instruments were deployed by 2017, one on the MetOp-A satellite and the other on MetOp-B. The MetOp satellites are part of the EUMETSAT Polar System (EPS), whose equator crossing time is 09:30 local time. MetOp-A was launched in October 2006. MetOp-B was launched in April 2013 to replace MetOp-A as the EPS's prime operational polar-orbiting satellite. Both satellites fly on the same orbit but are separated by 48.93 min (Munro et al., 2016). The third GOME-2, onboard the last of MetOp satellites, MetOp-C, has been launched in December 2018. It is designed to further improve the quality and frequency of the data. The corresponding GOME-2 products will come out in mid-2021 (https://directory.eoportal.org/web/eoportal/satellite-missions/m/metop).

With data from the aforementioned satellites, Georgoulias et al. (2019) compiled a dataset that's about 21 years long. Taking into account the different spatial resolutions of the different sensors, they took some steps to create a consistent dataset. First, Georgoulias et al. (2019) corrected for the low horizontal resolution of GOME, using a correction factor

generated from SCIAMACHY data. By taking the ratio of the original and smoothed SCIAMACHY data in the 9-year overlapping period, areas with constant high pollution levels will have a large ratio. Applying the ratio to GOME data helps to the polluted areas which are averaged out due to GOME's coarse resolution. When the ratio is applied to GOME data, highly polluted areas are emphasized when both datasets are sampled to the same resolution. Then, the corrected GOME data (GC1) was used to compare with SCIAMACHY data in the overlapping period to get a shift factor, which was later used to further correct GC1 for instrumental bias between the two sensors, generating GC2. The overall mean amplitude of each month of GC2 and SCIAMACHY data was used to correct for different seasonal amplitudes that may not be accounted for in GC1 or GC2, generating GC3. GC3 is the corrected GOME data to be used in the compilation.

OMI onboard NASA's Aura was launched in 2004. It has been monitoring atmospheric NO_2 at a much higher resolution than GOME (13 km × 25 km), but it has an afternoon crossing time. Considering the significant diurnal variability of NO_2 (Boersma et al., 2008), the OMI data were not used in Georgoulias et al.'s data compilation.

Using the compiled dataset, Georgoulias et al. (2019) studied trend changes in selected areas around the world. They showed that the NO_2 trends have reversed over large cities in the US, Western Europe, and Eastern China.

1.2. Statement of the problem

Unlike VCD measured by satellites, ground-level concentration of NO_2 is more relevant to public health. In the US, EPA's AQS (Air Quality System) has been collecting

ground-level NO_2 concentration since as early as the 1980s. EPA's network of AQS is mainly located in cities and urban agglomerations where a lot of human activities happen. Therefore, the EPA NO_x measurements are more representative of the urban environment. Even though the lifetime of tropospheric NO_x is short (~1 day against OH oxidation), and the concentration reported by AQS may not agree with the surface-level concentration derived from satellite tropospheric columns very well. Nitric oxide (NO) is a colorless gas which is difficult to observe from space, therefore only ground-level NO_2 is comparable to satellites and only NO_2 data are collected and analyzed for this research.

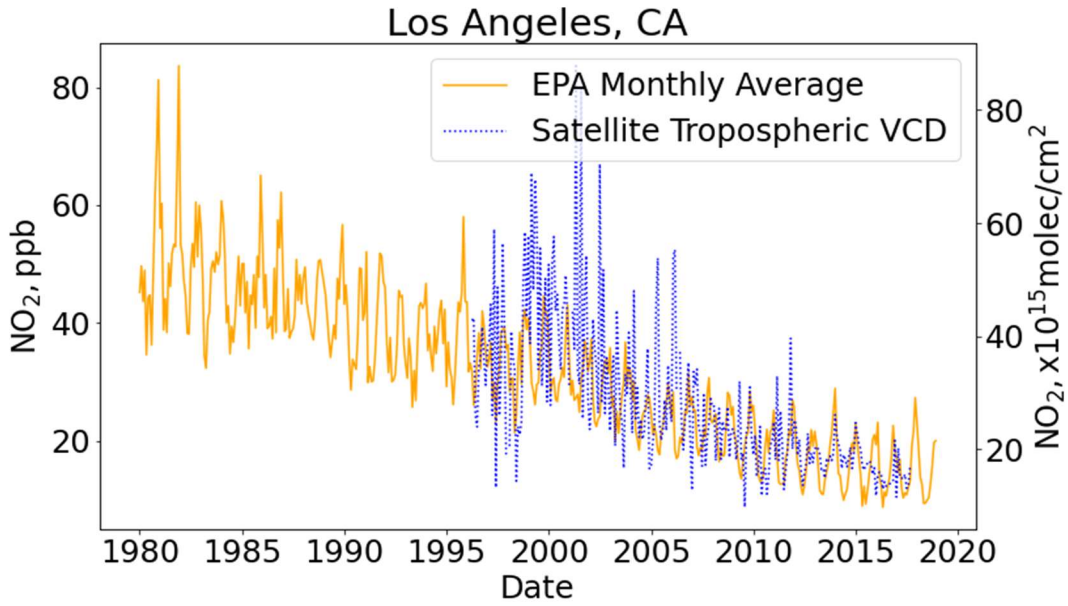

Figure 1-1 The EPA's data in Los Angeles, California shows a constant decrease over the 40-year period, while the satellite time series shows an increase before 2000 and a decrease afterwards.

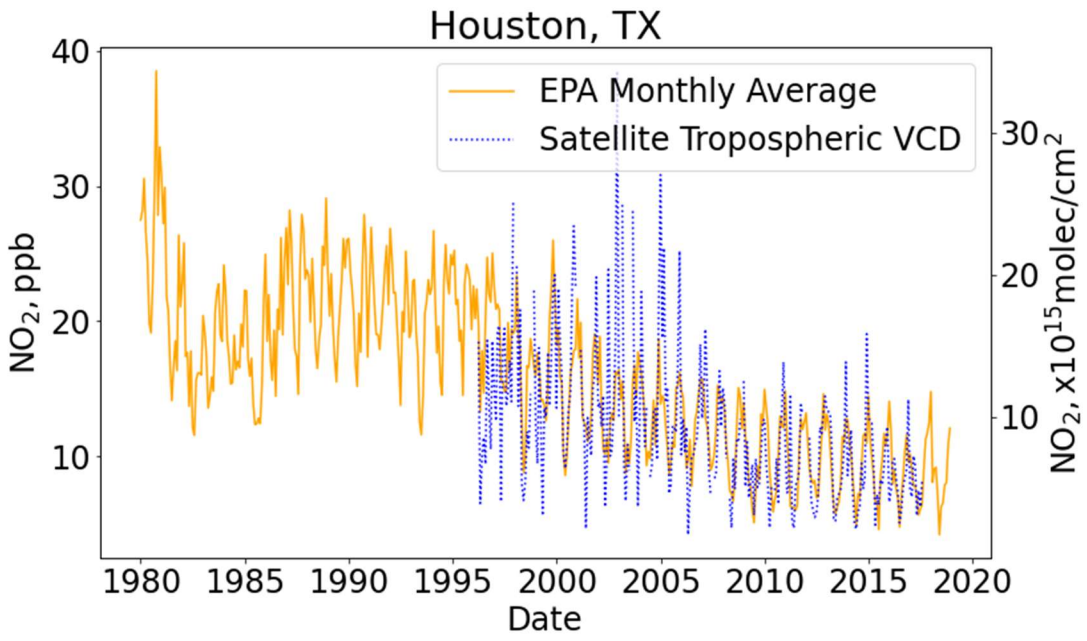

Figure 1-2 The trend reversal in Huston, Texas was not captured by the satellite time series.

Besides those in the US, Georgoulias et al. also found trend reversals in several regions in the world. For instance, the Iberian Peninsula in Europe showed trend change in about 2005.

Georgoulias et al. found trend reversals in several cities of the US, including Atlanta, Los Angeles, and San Francisco. No trend reversals were detected for Philadelphia, New York, Washington, D.C., and Huston. However, our preliminary studies show that cities having trend reversals showed no trend reversal in EPA's AQS data (also see Chapter 4). For example, the satellite time series showed a positive-to-negative trend change in Los Angeles, CA in 2000, but there does not seem to be a trend change even though ground-level data show a decreasing trend in the long term (Figure 1-1). In the meanwhile, trend

reversals were found for some other cities which was claimed to have no trend reversal (Figure 1-2).

In the preliminary data analysis, we analyzed EPA data in some major urban areas of the US, as well as European Environment Agency (EEA) data from major cities of EEA member countries. Using the methods described in Georgoulias et al (2019) and a few other studies, we investigate whether the change in NO_2 trend can be found in ground observations.

1.3. Organization of the Thesis

In Chapter 2, we review the EPA and EEA air quality data collection system, data format, and previous studies on the EPA data and the EEA data. In Chapter 3, we introduce the creation of an EEA NO_2 dataset which combines two periods of EEA data. After the selection of European cities for this study, we utilized the ECMWF in different ways to directly compare the ground station data and satellite data, then kept a smaller selection of European cities for trend change detection algorithm, which is introduced at the end of the chapter.

In Chapter 4, we discuss the diurnal and seasonal cycles in the EEA data, as well as the results of trend and trend change detection. The possible causes of the trend changes and the disadvantages of the trend change detection algorithm will be discussed in Chapter 5.

2 Dataset Review

2.1 Review EPA data

2.1.1 Studies using EPA NO_2 data

In the US, the human-induced NO_x emission estimation in 2011 was 14 Mt N, or 14 Pg N. It is quite high, considering the world anthropogenic NO_x emission in 1980 was 22 Tg N globally (https://www.epa.gov/sites/production/files/2017-05/documents/final_assessment_of_non-egu_nox_emission_controls_cost_of_controls_and_time_for_compliance_final_tsd.pdf).

EPA's AQS monitoring network adopts the EPA NO_2 chemiluminescence automated Federal Reference Method (FRM). Most NO_x-measuring instruments operate in two modes: In NO mode, NO reacts with O_3 to emit a luminescence which can be used to determine the concentration of NO; in NO_x mode, NO_2 is converted to NO using a converter, which is mainly MoO_x (molybdenum) catalyst heated to about 400°C. Then NO (original NO + converted NO) is converted to NO_2 and the emitted luminescence is measured. Taking the difference between NO_x mode and NO mode readings, one gets NO_2 concentration in the atmosphere. For photolytic converters, the heated MoO_x catalyst is replaced by a UV emitting device to induce NO_2 photolysis:

$$NO_2 + h\nu \rightarrow NO + O$$

The NO generated can then be converted to NO_2 by O_3 where luminescence intensity is proportional to NO concentration.

While the NO_2 records in EPA's Air Quality System (AQS) can date back to January 1980, their use for long-term NO_2 trend studies have been limited because of the sparseness and non-uniform distribution of air quality stations. Possible biases in NO_2 readings caused by MoO_x catalytic converters may also have made the use of these station data difficult: Not only NO_2 is reduced in those converters (e.g. MoO_x), but NO_z (reservoir) species, such as HONO and HNO_3 are also converted. Thus, NO_2 measured using chemiluminescence may be overestimated, especially in background regions where NO_x emission is low and NO_z is transported from nearby emission sources (Matthews et al., 1977; Ordóñez et al., 2006; Winer et al., 1974).

In Lamsal et al. (2015), NO_2 trend derived from EPA's AQS was compared to that derived from OMI tropospheric VCD. OMI has an afternoon passing time, therefore EPA hourly data between 13:00-15:00 was used in the study. After removing stations that ceased operation between 2005-2013, 208 sites remained. The trend analysis showed an average reduction of 37.7±5.4% over all stations. A time series measured by a photolytic converter NO_2 analyzer at a rural site in Yorkville, Georgia was used to compare with that measured by a MoO_x converter in the same area. There were larger biases in 2010 compared to 2005, and MoO_x instruments were more biased in afternoon hours compared to morning hours.

Zhang et al. (2018) used the EPA NO_2 as "ground truth" when analyzing long-term trends in original and improved OMI NO_2 data. They used Mann-Kendall method with Sen's slope estimator to calculate the relative trend of NO_2 for each season (DJF, MAM,

JJA, SON) from 2005 to 2014. OMI product using DOMINO v2 algorithm. Mann-Kendall method is a non-parametric test where each point is compared with all preceding points to determine whether there is a trend in the time series. Their study focused on correcting OMI data using lightning data and MODIS surface albedo to match with AQS data.

Previous studies have attempted to use ground-based NO_2 measurements to evaluate OMI's tropospheric NO_2 column retrievals (Dunlea et al., 2007; Lamsal et al., 2008; Steinbacher et al., 2007). Ground-level NO_2 concentrations were derived from satellite column retrievals, which will also be attempted in this study. Since EPA's AQS data were used for validation, an algorithm was developed to correct for the interference with NO_2 mixing ratios measured by MoO_x converters (Lamsal et al., 2008, 2010, 2013, 2014).

2.1.2 Data format and contents

EPA data used in this study are all pre-generated datasets and are all in Comma Separated Value (.csv) format. Both daily and hourly data are used.

The daily data product we use is called "daily summary files", and the hourly data we use is called "hourly data files". Most EPA monitors make one measurement per hour, and in the "daily summary" files are the NO_2 arithmetic mean of all qualifying observations in a 24-hour period. The daily summary contains data for every monitor in the EPA database. If the monitor only takes one sampler in a 24-hour duration, that value will be used as the daily summary record and will not be included in the hourly dataset.

Both daily summary dataset and hourly dataset are separated into smaller files by the year of observation and parameter (e.g. O_3, SO_2, NO_2). For stations with more than one

NO_2 monitor, hourly data from each monitor is recorded, and can be distinguished by "Parameter Occurrence Code" ("POC"), "Method Code" and "Method Name".

Both EPA datasets, in the form of tables, contain a lot of fields. And a lot of them are redundant for this research. For all NO_2 observations by EPA, the "Units of Measure" is ppbv; since all data is NO_2, the "Parameter Name" (NO_2) and "Parameter Code" do not change with the station. For NO_2, the EPA Parameter Code is 42602. In the EPA monitor and site listing files, the location setting (urban, suburban, rural) and land use (residential, agricultural, commercial…) are described, which can be used to study a specific kind of station. For the description of other research-related fields in the csv table, please refer to Appendix 1.

2.2 Review EEA data

2.2.1 EEA previous studies

The European Environment Agency (EEA) has 32 member countries (as of October 2020). As an agency of the European Union (EU), its goal is to help improve Europe's environment by providing timely and reliable information. The European environment information and observation network (Eionet) is a partnership network of the EEA and its member and cooperating countries. The member and cooperating countries are bound under Decision 97/101/EC to exchange air quality information. By the Exchange of Information (EoI) procedure, each station has a unique reference code (EoI code). The stations are also classified and labelled according to Decision 97/101/EC, so that one can tell their area type from the metadata or the data table.

Two datasets from two versions of EEA's air quality database are used in this study: AirBase v8 and Air Quality e-Reporting (AQ e-Reporting). Both datasets contain multi-annual time series of air quality measurements, corresponding statistics, and air quality stations' metadata. AirBase v8 is the name of the dataset collected before 2013, hence referred to as BEF2013 from now on; Air Quality e-Reporting is referred to as AFT2013 from now on. AFT2013 consists of datasets E1a and E2a, tested by automated quality check. For more information, please refer to Appendix 1.

Unlike EPA's AQS data, academic studies using EEA's AirBase data are very limited, and to our knowledge, there has not been any study using a complete EEA dataset. The reason for this limited usage of the EEA data may be the difficulty to compare NO_2 changes caused by different policies and economic factors of different countries across the EU. Since EPA NO_2 data have been used in previous studies but EEA NO_2 data have not been widely used to date, this thesis will examine the EEA data quality for academic use.

Previous studies have examined the NO_2 trends over individual cities (Gualtieri et al., 2014; Mangia et al., 2011), compared NO_2 trends in several cities (Henschel et al., 2013, 2016; Keuken et al., 2009) and used only one dataset to do pan-Europe NO_2 trend analysis (Chen et al., 2019; Guerreiro et al., 2014). Like studies using EPA data, the issue with chemiluminescence analyzers using catalytic converters was also addressed in the studies using EEA data.

In general, the NO_2 level in the EU has dropped significantly since the 2000s. In the period 2002 to 2011, it was estimated that NO_x emission in the EU dropped by 27%. The transport is the major emission sector; the next largest source of NO_2 is the energy

sector. EEA sets a standard that annual NO_2 mean should be below 40 $\mu g/m^3$, and should not exceed 200 $\mu g/m^3$ for more than 18 times a year (https://www.eea.europa.eu/themes/data-and-maps/figures/air-quality-standards-under-the). These limits are often exceeded, often over stations that are located by the roadside traffic (TR) (Guerreiro et al., 2014; Henschel et al., 2016).

2.2.2 Data format and contents

Product description , metadata, and BEF2013 download link for each country can be found at: https://www.eea.europa.eu/data-and-maps/data/airbase-the-european-air-quality-database-8.

Files containing observations are called "raw data files", which are located in the "/raw" folders in the zip files. Raw data are tab-delimited text files containing date and time (for hourly data) of observations as well as the corresponding quality flags. For daily data, each row has data of all days in one calendar month; for hourly data, each row has data for all hours in one calendar day. Quality flags less than or equal to 0 indicate invalid or missing data.

The zip files for each country also contain the metadata of the monitoring network. The "stations.csv" table includes the European code, station local code, longitude, latitude, city, station name, station start/end date, station type, area type, etc. These data, especially the station longitude and latitude, will later be used to help concatenate BEF2013 and AFT2013 into a single dataset. The "Measurement_configurations.csv" table includes different components and corresponding component codes, as well as measurement unit, sampling frequency and measurement technique principle.

Member countries of EEA may have their own naming conventions for the stations. In EEA, the EoI code is used to identify the stations. The file names of BEF2013 contain EoI code, pollutant code (00008 for NO_2), and data type (daily, daily maximum ("dymax"), 8-hourly and hourly). That information can be used to find station type and longitude and latitude in the "stations.csv" tables.

For AFT2013, one can build request URLs to download the data from https://discomap.eea.europa.eu/map/fme/AirQualityExport.htm. Each URL points to one file, and usually one file corresponds to one monitoring station. Columns relevant to this study are station local ID ("AirQualityStation", "AirQualityStationEoICode"), station measurements ("Concentration"), measurement time ("DateTimeBegin", "DateTimeEnd") and quality flags ("Validity", "Verification"). For quality flags, "Validity" must equal to 1 for the data point to be valid and above instrument detection limit (http://dd.eionet.europa.eu/vocabulary/aq/observationvalidity/view); "Verification" must be equal to 1 to be "verified". For the verification flag, 2 means "preliminary verified" and 3 means "not verified".

Longitude and Latitude of the stations can be retrieved from station information files using station local IDs. For more details, please refer to Appendix 1.

In both BEF2013 and AFT2013 datasets, air quality stations are given an "area type" and a "station type". Area types may be "urban", "suburban" and "rural", and station types may be "traffic", "industrial" and "background". In this study, although all those data were processed, only background stations in urban and suburban areas were used for analysis. In the EEA's definition, "suburban" areas are "largely built-up", and can be suburban on

their own without any “urban” part. Therefore, suburban areas are treated as urban areas in this study.

3 Methods

3.1 Data Processing

Since EEA data are separated into a pre-2013 dataset (BEF2013) and a post-2013 dataset (AFT2013), either needs to be treated specifically before concatenation.

The quality flags in BEF2013 were used to remove unqualified measurements. Quality flag QA = 0 means the value in that hour is invalid, and the measurement value is to be filled in by a large negative number –999. Thus, both either QA = 0 or value = –999 represents an invalid observation.

For AFT2013, “Verification” and “Validity” are necessary fields to filter out invalid data; The flag “AveragingTime” = “hour” is also needed to make sure that the extracted data points correspond to hourly measurements instead of daily. For BEF2013, hourly data and daily data are in different files, so the identification is more straightforward.

For more detailed information in processing of EEA datasets, please refer to Appendix 2.

3.1.1 Dataset Generated

3.1.1.1 EEA station information

EEA station information is stored in tables for both BEF2013 and AFT2013. The two tables were merged using the unique longitude and latitude of the stations, rounded to the third decimal place. The methods, area types and station types were string fields and were all converted to lowercase.

3.1.1.2 Station-wise monthly mean of hourly mean (SMA)

The output data are in the form of .nc (NetCDF4) file. Variables in the final output file are: ['longitude', 'latitude', 'date', 'hour', 'no2']. In the file, "date" and "hour" are fixed dimensions. "Date" variable is the number of days since 1970-01-01, to include some stations which started to collect data in the 1970s. There are 556 months in total. The months containing no data will be filled with NaNs. Dimension "hour" has a size of 24.

Longitude ("lon") and latitude ("lat") can be used to retrieve station information. Station type and area type can be retrieved from the merged "EEA station information" csv files, using longitude and latitude range as the reference.

Dimensions of the NO_2 variable are [station index, hour, date]. The "station index" dimension is aligned with longitude and latitude variables, so the indices of longitude and latitude values can be used to retrieve NO_2 data of corresponding stations. Without merging, there are 8817 records for "index", hence also for "longitude" and "latitude".

3.1.2 Satellite data

Georgoulias et al. (2019) archived their composite NO_2 satellite data at the Tropospheric Emission Monitoring Internet Service (TEMIS): https://d1qb6yzwaaq4he.cloudfront.net/airpollution/no2col/GOME_SCIAMACHY_GOME2ab_TroposNO2_v2.3_041996-092017_temis.nc. The file is a NetCDF4 file with the following variables: ['lon', 'lat', 'time', 'TroposNO2']. Tropospheric NO_2 data layers were binned into 0.25°×0.25° longitude-latitude grids, and were stacked along the time dimension. The dataset contains NO_2 data from April 1996 to September 2017 (258

months), and 'TroposNO2' variable has a dimension of (258, 720, 1440). Longitude and latitude of the cities can be used to retrieve the corresponding time series along the time dimension.

3.2 Selection of cities to study

A number of cities were selected for this study. The selection of cities was based on the following criteria:

1. High pollution levels. Due to the high-bias in some chemiluminescence NO_x analyzers, the higher the NO_2 level, the smaller the relative error and therefore the closer the reading is to the actual NO_2 level. An example of a "good" month with good satellite NO_2 data coverage over the EU was October 1996 (Figure 3-1), where there was high NO_2 levels near the English Channel and in the south of the Alps.
2. Distant from one another. If the cities selected are scattered across the European continent, the NO_2 trends are less likely to be affected by a nearby pollution source.
3. It needs to be a city with multiple stations. With more stations, the NO_2 data are collected from different parts of a city and is less likely to be affected by a single pollution source.
4. Long NO_2 record. This is important to test whether the trend changes reported in Georgoulias et al. (2019) is robust or not.

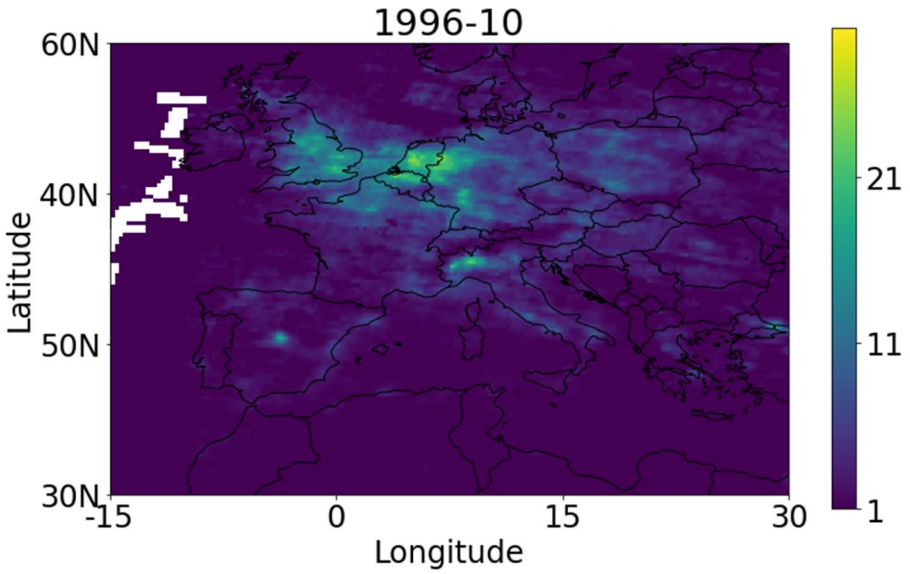

Figure 3-1 One slice of monthly average data from the Georgoulias's NO_2 dataset showing the NO_2 hotspots in the Europe.

Large cities are more likely to satisfy above criteria. Capital cities are usually large cities with multiple stations, and are more likely to be the first cities to set up air quality stations in the country.

For this study, we selected 24 cities in the EU (Table 3-1, Figure 3-2). When retrieving EEA time series from the SMA file, stations in a 0.25°×0.25° bounding box around a city center were selected. The central geo-coordinates of the bounding boxes were the coordinates of the city title when viewing them on Google Earth.

London, UK	Birmingham, UK	Glasgow, UK
Hamburg, Germany	Berlin, Germany	Munich, Germany
Dusseldorf, Germany	Rotterdam, Netherlands	Madrid, Spain

Barcelona, Spain	Lisbon, Portugal	Paris, France
Lyon, France	Geneva, Switzerland	Zurich, Switzerland
Rome, Italy	Milan, Italy	Bologna, Italy
Vienna, Austria	Warsaw, Poland	Budapest, Hungary
Prague, Czech Republic	Athens, Greece	Brussels, Belgium

Table 3-1 A list of the 24 cities selected for the analysis of NO_2 trend

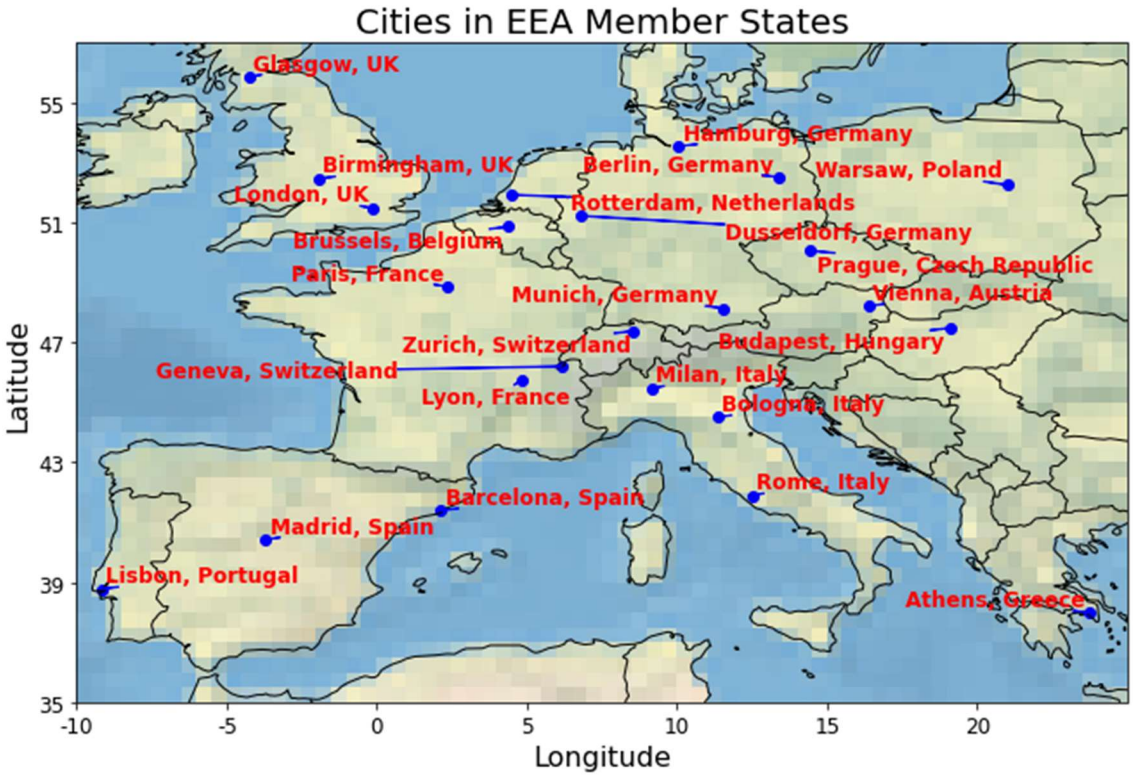

Figure 3-2 A map of the 24 cities selected for the analysis of NO_2 trend

3.3 Estimating NO_2 column density

There are two ways to compare satellite data with ground-level measurements. We can either convert tropospheric column density to concentration near the surface, or convert

concentration near the surface to tropospheric column density. Either way, a prior NO_2 vertical profile is needed in the conversion.

We use the NO_2 vertical profile from ECMWF CAMS global reanalysis (EAC4) monthly averaged fields, accessible via the climate data store (CDS) API: (https://ads.atmosphere.copernicus.eu/cdsapp#!/dataset/cams-global-reanalysis-eac4-monthly?tab=overview).

The CAMS reanalysis is the latest atmospheric composition product from the Copernicus Atmosphere Monitoring Service, produced using 4DVar data assimilation in ECMWF's Integrated Forecast System (IFS). It has 60 model pressure levels, with the top level at 0.1 hPa. In monthly averaged fields, the pressure levels are interpolated to 25 pressure levels, from 1000 hPa to 1 hPa.

Since CAMS reanalysis NO_2 profile product start only from 2003, it is impossible to compare satellite and ground-level NO_2 from 1996 to 2003. Our approach is to compare the CAMS-converted vertical NO_2 column over the common period (2003–2017) and select cities where the CAMS-converted and satellite vertical NO_2 column agree well. The selected cities can then be used as proxies for the vertical NO_2 column before 2003.

The ground-level measurements from EPA are unitless (mixing ratio, ppb), and that from EEA are in the unit of $\mu g/m^3$ (mass concentration). But ECMWF's NO_2 variable is in the unit of mass mixing ratio (kg/kg). We used the molar mass of air and NO_2 (μ_{air}=29 g/mol and μ_{NO2}=46 g/mol) to convert ECMWF's data (m_{NO2}) to volume mixing ratio:

$$c_{NO_2} = m_{NO_2} * \mu_{air}/\mu_{NO_2}$$

Then, we replaced the surface level of ECMWF NO_2 profile, and integrated over the adjusted ECMWF profile in the troposphere (1000 hPa to 200 hPa) to get a column density time series which can be used to compare with the satellite observations.

The column density (in the unit of molecules/cm^2) is the integral of number density (in the unit of molecules/m^3) over an altitude interval (in meters) and divided by $10^4 cm^2/m^2$:

$$D = \int_{z1}^{z2} c_{NO_2} N_{air}\, dz$$

where c_{NO2} is volume mixing ratio and Nair is the number density of air. Here $N_{air} = \frac{\rho_{air} N_{Av}}{\mu_{air}}$, where N_{Av} is the Avogadro's number, 6.02214×10^{23}/mol; and $dz = -\frac{dp}{\rho_{air}\, g}$, where g = 9.8 m/s^2. Thus we have:

$$D = -\int_{p1}^{p2} m_{NO_2} \frac{\mu_{air}}{\mu_{NO_2}} \frac{\rho_{air} N_{Av}}{\mu_{air}} \frac{1}{\rho_{air} g}\, dp$$

Here ρ_{air} is cancelled out. Taking the negative sign into account, and we get:

$$D = \int_{p2}^{p1} \frac{m_{NO_2} N_{Av}}{g\, \mu_{NO_2}} dp$$

Figure 3-3 compares the ECMWF profile with ECMWF profile using ECMWF for the surface level ("modified" ECMWF) and with the satellite time series.

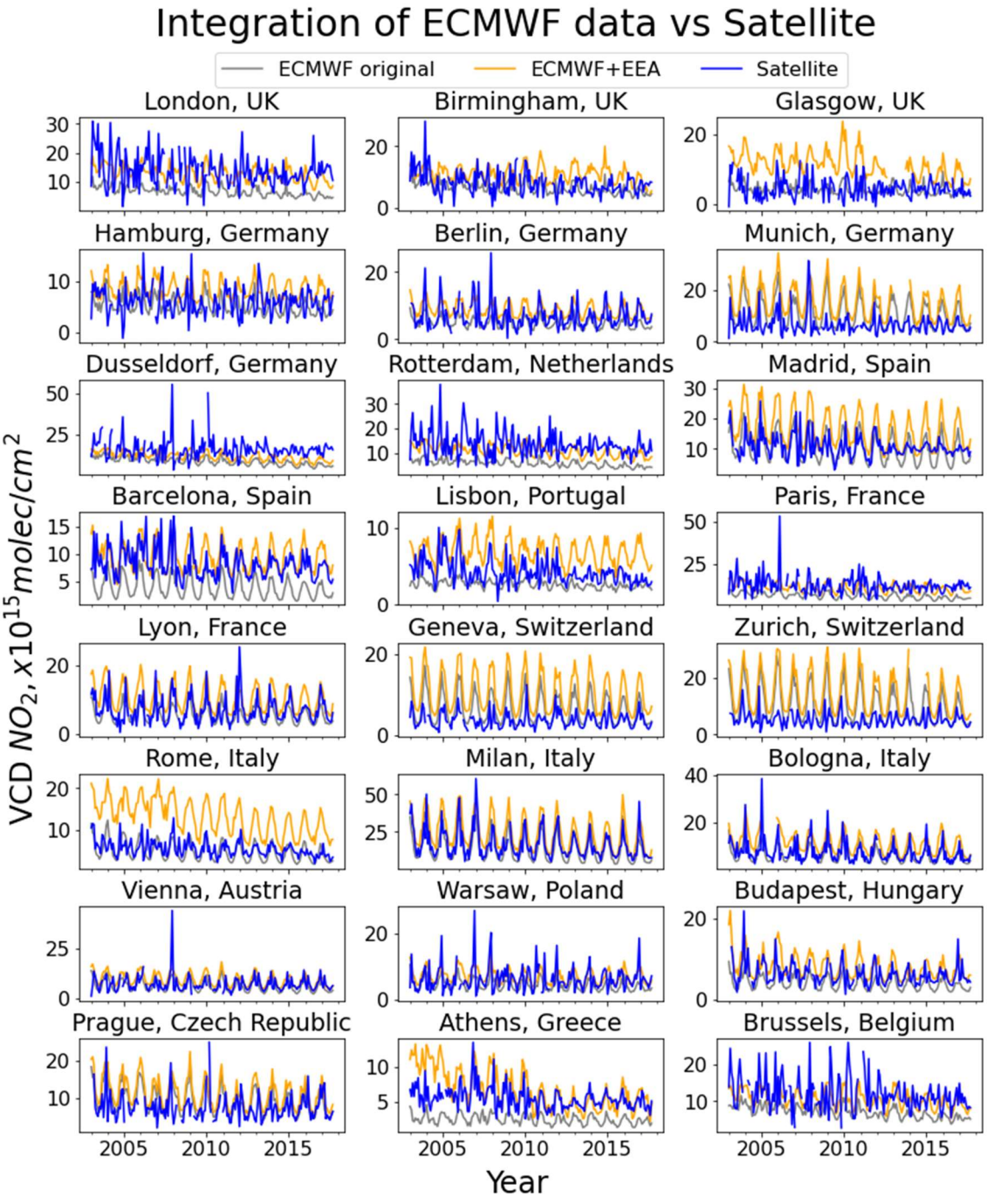

Figure 3-3 Comparison of the integrated ECMWF reanalysis data, the ECMWF reanalysis data with EEA data as the surface level, and the satellite data. The integrated ECMWF reanalysis data do not match the satellite observations in many cities.

The difference between ECMWF and satellite data turned out to be small in many cities: Birmingham (UK), Hamburg (Germany), Berlin (Germany), Lyon (France), Milan (Italy), Bologna (Italy), Vienna (Austria), Warsaw (Poland), Budapest (Hungary), Prague (Czech Republic). In some cities, the integrated NO_2 column density using modified ECMWF was much higher than that created using the original ECMWF NO_2; in Glasgow (UK), Lisbon (Portugal), Rome (Italy) and Athens (Greece), the trend is also noticeably different.

The ECMWF data has a lower spatial resolution than the satellite data and would very likely smooth out the pollution hotspots that are seen by satellites. Thus, we generally expect a lower column density in ECMWF than in the satellite data. Figure 3-3 shows that the tropospheric column density in Munich (Germany), Geneva (Switzerland) and Zurich (Switzerland) are much higher than that from the satellite and are therefore counterintuitive.

Directly comparing the ECMWF column density and surface concentration with the satellite data (Figure 3-4), we notice overestimation of NO_2 level in the ECMWF Reanalysis dataset over Switzerland, Southeastern France, Southern Poland, Slovakia, Czech Republic, and Austria in January 2005.

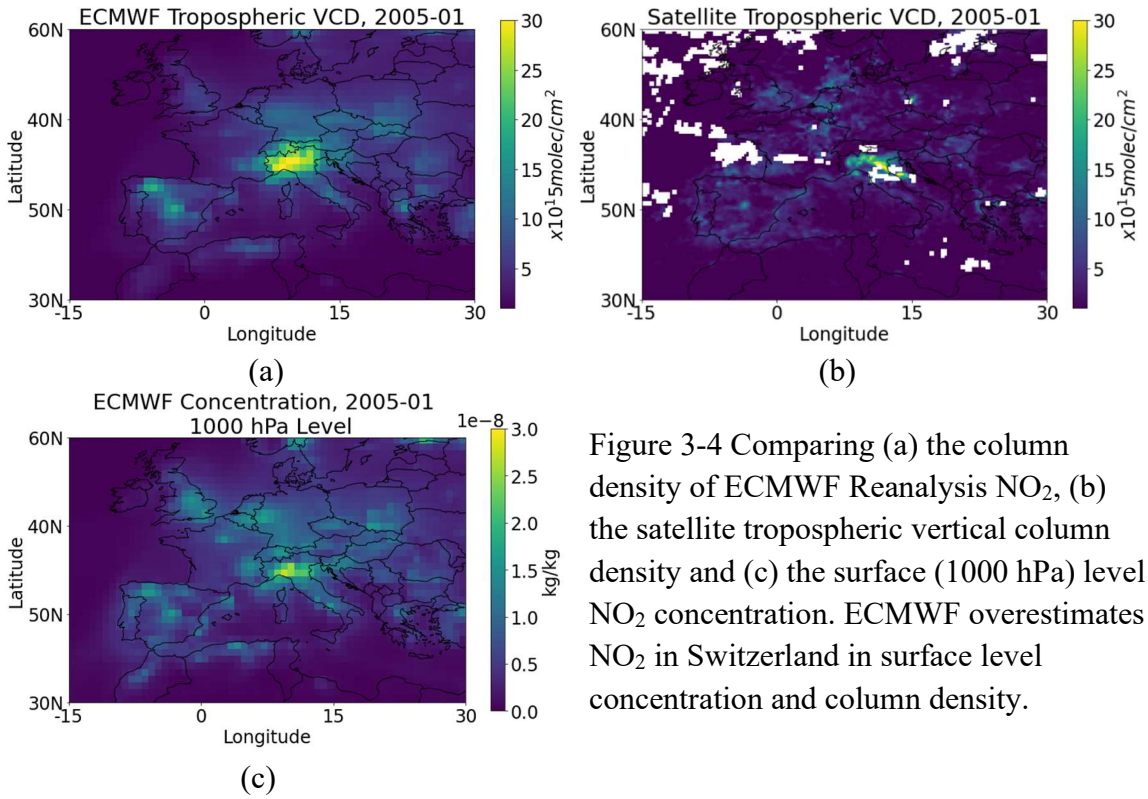

Figure 3-4 Comparing (a) the column density of ECMWF Reanalysis NO_2, (b) the satellite tropospheric vertical column density and (c) the surface (1000 hPa) level NO_2 concentration. ECMWF overestimates NO_2 in Switzerland in surface level concentration and column density.

The overestimation in the ECMWF NO_2 over these areas and cities may be due to subgrid processes that are beyond the scope of this thesis. Instead, our purpose is to validate the satellite NO_2 trends using station measurements, which we achieve by picking locations where ECMWF/station NO_2 column and satellite retrievals agree. Thus, in the trend and trend change analyses, the cities where ECMWF and satellite data do not match well will be excluded. Cities to be excluded are: London (UK), Munich (Germany), Barcelona (Spain), Geneva (Switzerland), Zurich (Switzerland) and Athens (Greece). Figure 3-5 shows a map without the 6 cities.

Figure 3-6 compares the seasonal cycles of original ECMWF NO_2 column and the ECMWF-station combined NO_2 column. In this step, the seasonal cycles were taken as the mean of corresponding months over the whole time series.

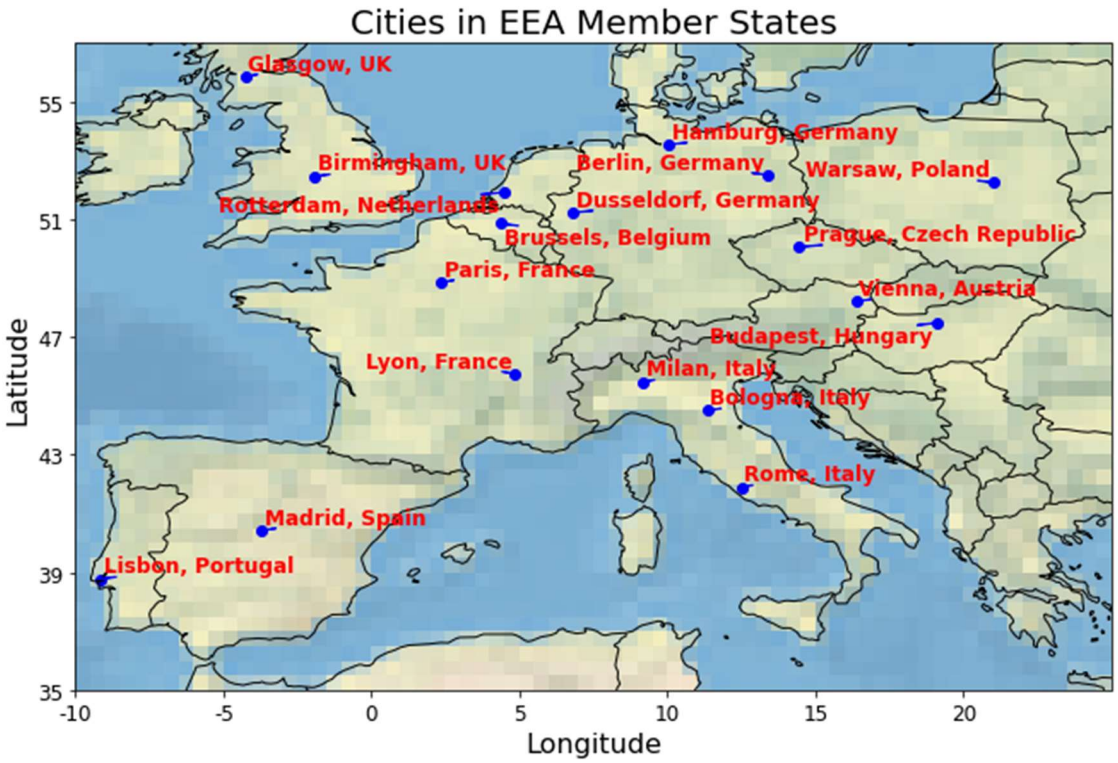

Figure 3-5 A map of the 18 cities selected for the analysis of NO_2 trend. The cities where ECMWF and satellite data do not match well are excluded.

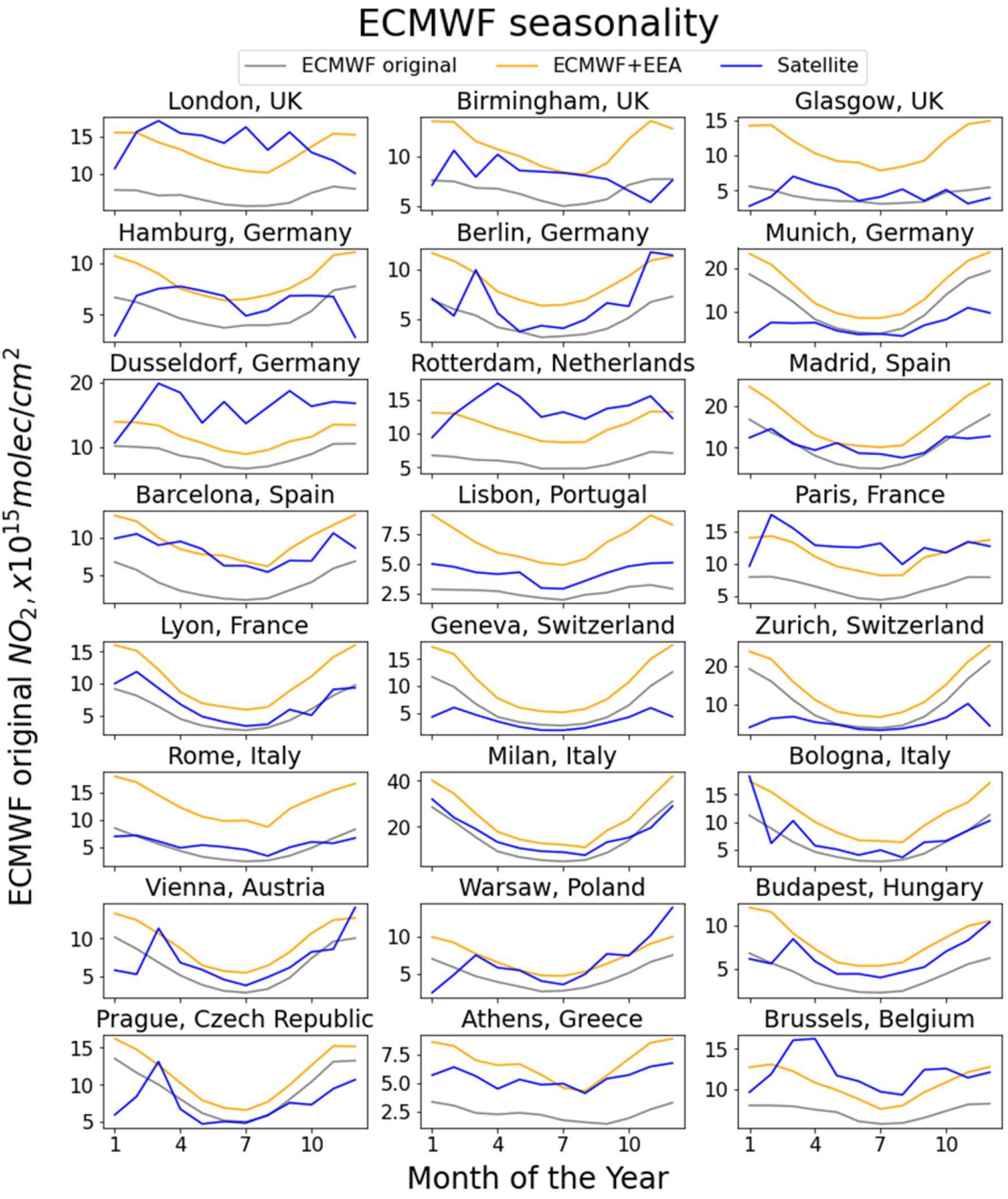

Figure 3-6 Comparing the seasonal cycles of original ECMWF, modified ECMWF and the satellite time series. The seasonal cycles were computed from the whole overlapping time span, from January 2003 to March 2017.

In regard to the mean seasonal cycle, the original ECMWF NO_2 column density is always lower than the column density from the ECMWF-station combined product. Due to the decrease in boundary layer height and in the photolysis of NO_2 during the winter, the tropospheric column density of NO_2 is higher, as can be seen in both the reanalysis data and the satellite data. However, the mean seasonal cycle of the satellite NO_2 column is generally not sinusoidal, in contrast to the assimilated NO_2 column. In particular, the satellite-retrieved NO_2 column in February to April over some cities is higher than that in December and January, a temporal behavior that is not seen in the reanalysis data. Peak in February to April in satellite data is the most significant in Berlin (Germany), Rotterdam (Netherlands), Paris (France), Vienna (Australia), Budapest (Hungary), Prague (Czech Republic) and Brussels (Belgium). Also noticeable is the low or even reversed seasonality in some cities, such as London (UK), Hamburg (Germany) and Dusseldorf (Germany). This is likely caused by the outliers in the time series, such as the spike in Paris (France) in 2006 and in Vienna (Austria) (Figure 3-3). Since we do not know the cause of those outliers, we could not design a way to remove them from the time series.

3.4 Estimating ground-level NO_2 concentration

For consistency, we also derive surface NO_2 concentration inversely from satellite retrievals, again using ECMWF vertical profile. The difference in the spatial resolutions of ECMWF and satellite retrievals are taken into account using the method described in (Lamsal et al., 2008, 2010, 2013, 2014). The method assumes that NO_2 in the planetary boundary layer (PBL) is well-mixed, so one can use ECMWF data for the ratio of PBL

NO_2 against the free troposphere and the whole column. Then the ratio is applied to satellite retrievals [i.e. the dataset from Georgoulias et al. (2019)] to get an estimation of satellite-based PBL mixing ratio. This approach compares ground station or satellite-derived surface level mixing ratio or concentration.

$$S = \left[v + (v+1) \frac{\Omega_{E,free}}{\Omega_{E,PBL}} \right] \frac{S_E}{\Omega_E} \Omega_{Sat,Box}$$

Here, S_E is the modeled NO_2 concentration (ECMWF in this study) at surface level, Ω_E is the NO_2 column density over the whole troposphere and $\Omega_{E,PBL}$ is the NO_2 column density in the PBL. The difference in the spatial resolutions is taken into account by taking the ratio $v = \frac{\Omega_{Sat}}{\Omega_{SatBox}}$, where Ω_{Sat} is the satellite column density and $\Omega_{Sat,Box}$ is the mean satellite column density in the area of the model which provides the NO_2 profile. Here the horizontal variation in free-tropospheric NO_2 columns ($\Omega_{E,free}$) is assumed to be negligible, because NO_2 has a longer lifetime in the free troposphere. The ECMWF dataset is in 0.75° grids, and the satellite dataset is in 0.25° grids. One ECMWF grid contains exactly 9 satellite pixels, thus there is no need for interpolation when retrieving $\Omega_{Sat,Box}$.

Since NO_2 in the PBL is assumed to be well-mixed, we need the PBL height to determine the altitude (pressure level) to which the NO_2 from ground-level measurements can represent, and get $\Omega_{E,PBL}$. In the ERA5 dataset from ECMWF, the PBL height variable is on "single levels", in the "other" section. We used the monthly averaged PBL height to match with the NO_2 data (https://cds.climate.copernicus.eu/cdsapp#!/dataset/reanalysis-

era5-single-levels-monthly-means?tab=form). The 2m temperature and surface pressure product of ERA5 were also used to convert the PBL height from altitude (meters) to estimated pressure level (Pascal).

Another way to determine the PBL height Relative humidity (RH) data is one of the fields in EAC4 monthly averaged fields product, but it only has data at pressure levels such as 1000 hPa, 950 hPa, 925 hPa, 900 hPa, 850 hPa, etc. It is too sparse to determine the boundary layer height solely based on the EAC4 data.

EEA data is converted to ppb using the surface temperature as the reference. The surface temperature data used in this conversion is from ECMWF EAC4. The dataset came with temperature at multiple data pressure levels in every three hours. We used this dataset to be more persistent with the EAC4 NO_2 profile from ECMWF.

The NO_2 concentration at surface level estimated using Lamsal et al.'s method is quite different from what is observed by EEA (Figure 3-7). In the meanwhile, the selected stations (i.e. ECMWF and satellite NO_2 agree) in the previous section also show discrepancy. As a result, also considering the short temporal coverage of the dataset, the ECMWF's NO_2 will not be useful to trend reversal detection.

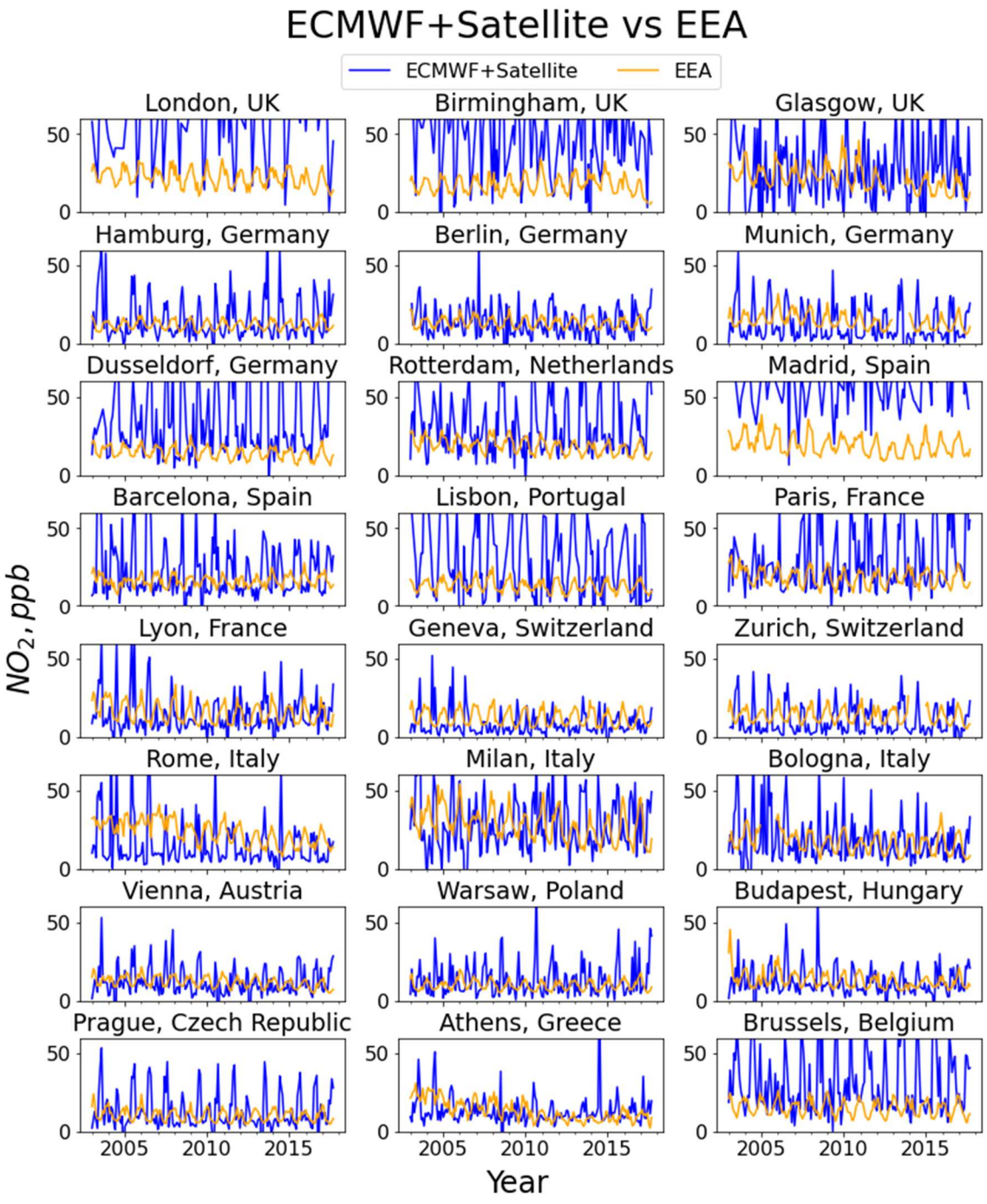

Figure 3-7 Combining the satellite data and the ECMWF profile to generate the surface level concentration and compare with the EEA data. The estimated surface level concentration is too large in comparison.

3.5 Diurnal cycle and seasonal cycle

Using the EEA SMA product, we can assess the diurnal cycle and the seasonal cycle in the NO_2 time series. In this study, we used 5-year arithmetic mean for both cycles, so that the change in diurnal & seasonal cycle through time can be easily observed on the plot and is less affected by noise in some of the years.

3.6 Trend analysis

The trend analysis model in this study was also used by Georgoulias et al. (2019) and was based on a method described in Weatherhead et al. (1998); the trend change detection was based on the model used for trend analysis.

The trend analysis model uses a linear regression with a seasonal component. With up to 6 periods per year, the model can capture both the trend and the seasonality.

$$Y_t = A + BX_t + \sum_{n=1}^{6}\left[a_n sin\left(\frac{2\pi}{T}nX_t\right) + b_n cos\left(\frac{2\pi}{T}nX_t\right)\right] + N_t$$

Here Y_t is the monthly mean value for month t, and X_t is an ordinal value (0,1,2…) for the month in the whole time series (X_t). From the regression, we get A as the intercept, B as the slope, the linear trend, and N_t as the residual, or the remainder. In this study, T, the period, is set to be 12 to match with the annual NO_2 variability.

To include the possible effects of unknown or unmeasurable natural factors which makes N_t vary smoothly over time, here we assume N_t to be autoregressive of the order of 1, and it is stationary so that the autocorrelation in the residual, φ , has $-1<\varphi<1$:

$$N_t = \varphi N_{t-1} + \varepsilon_t$$

Here ε_t is the white noise.

The standard deviation of the residual, σ_N, along with φ and the number of years of data, m, can be used to approximate the standard deviation of the trend B:

$$\sigma_B \approx \frac{\sigma_N}{m^{3/2}} \sqrt{\frac{1+\varphi}{1-\varphi}}$$

The trend B is considered statistically significant at the 95% level if $|B/\sigma_B| > 2$.

In this study, to avoid the influence of fluctuations in traffic amount and road condition, only the background stations in urban (and suburban) areas were used. NO_2 trends in the urban background (UB) stations are compared with traffic (TR) stations in the trend analysis.

3.7 Trend reversal detection

The method used in this study to detect the change point in a time series was introduced in (Cermak et al., 2010). This method is a moving window detection, where two

neighboring five-year windows moves along the time series and the following metric is computed for both windows:

$$S(t) = \frac{\min\{(p(B_l), p(B_r)\}}{|B_l - B_r|\,\sigma_{Bc}}$$

For any data point in the middle of the time series, we calculate the trend B_l in the 5-year window on the left of the data point; similarly, we also calculate the trend B_r in the 5-year window on the right of the data point. A score S(t) can be constructed by taking the smaller p-value of B_l and B_r, divided by the absolute difference $|B_l - B_r|$ and the standard error of the trend for left and right window combined σ_{Bc}. Here standard error σ_{Bc} is computed with the method described in section 6, and c=(l+r) is the combined left and right window. S(t) is obtained at all data points (except the 5 years at the left and right edges). The minimum value of S(t) would be at a data point where the p-value of trends in either the left or the right window is relatively small, the absolute change in trend is relatively large, and the standard error of the combined periods is relatively large. Thus, the data point at which S(t) is minimum is a candidate of statistically significant trend change.

To make sure only trend reversals are detected, only the data points where B_l and B_r are of different signs were analyzed, and S(t) is set to not-a-number (NaN) if neither B_l nor B_r are significant. Only years with more than 8 months of valid data were considered when detecting trend reversal.

4 Results

4.1. Comparing traffic and background; EEA vs Sat, long term trend

We used the regression model described in chapter 3 to extract the linear trend in NO_2. The multi-year NO_2 linear trend from urban-background stations (UB) and traffic stations (TR) in each city, along with that from the satellite time series, are shown in Figure 4-1. The amplitudes and the trends over the urban-background and traffic stations are quite different. The trends over traffic stations showed much stronger decreases compared to the urban-background stations in Rome (Italy), Bologna (Italy) and Warsaw (Poland), where the annual decrease of NO_2 over the traffic stations are more than 2 times those over the urban-background stations. Some traffic stations have shown an overall increase over the years: Hamburg, Berlin, and Dusseldorf in Germany. Even though the trends over urban-background stations and traffic stations can be similar, the pollution levels of NO_2 are usually different. For instance, the trend in Vienna, Austria in the urban-background is –0.482 μg/(m^3 year), and trend over traffic stations is –0.64 μg/(m^3 year), but the mean NO_2 level over traffic stations is slightly above the 40 μg/m^3 standard while the mean NO_2 over urban-background stations is below it.

The availability of urban-background stations and traffic stations data can be very different as well. In Birmingham, UK, the traffic stations only started recording after 2015, while urban-background stations have been providing data since the late 1980s. Besides, the traffic stations mainly capture pollutants from road traffic, and may not represent the

well-mixed surface level air in urban areas. Therefore, only urban-background stations are used for the rest of the analyses in this study.

Due to the precision of SCIAMACHY, Georgoulias et al. (2019) ignored trends that are below 0.1×10^{15}molec/cm^2 per year. If we follow their selection criterion, the NO_2 trends in the following cities are not significant: Berlin (Germany), Lisbon (Portugal), Lyon (France), Bologna (Italy), Vienna (Austria), Warsaw (Poland) and Budapest (Hungary).

Most EEA time series are longer than satellite time series. Exceptions are Paris (France), Rome (Italy), Milan (Italy) and Bologna (Italy).

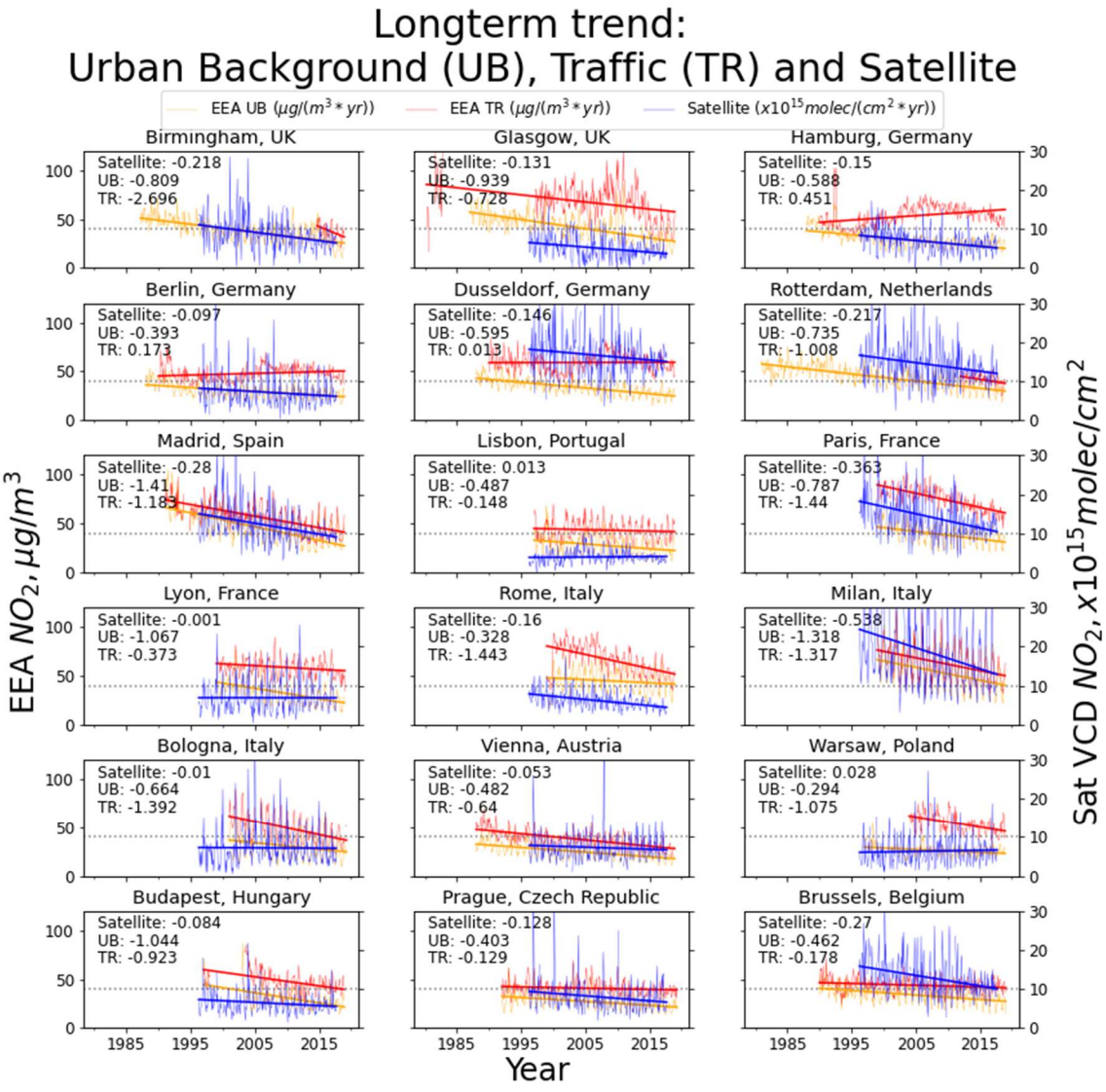

Figure 4-1 Comparing the long-term NO_2 trend in traffic stations, urban background stations and the satellite.

4.2. The overall trend

The seasonality in time series can be removed by the seasonal decomposition function in Python "statsmodels" library. Since the EEA time series may contain missing values, I used a moving window average function with a window size of 12 months to remove the seasonal cycle instead. The deseasonalized NO_2 time series over the selected EU cities has a decreasing trend, and most cities are approaching or are already below the 40 μg/m^3 annual NO_2 limit by 2019. Interestingly, a slowing decrease or even a trend reversal can be seen over the cities that had EEA records before the mid-1990s.

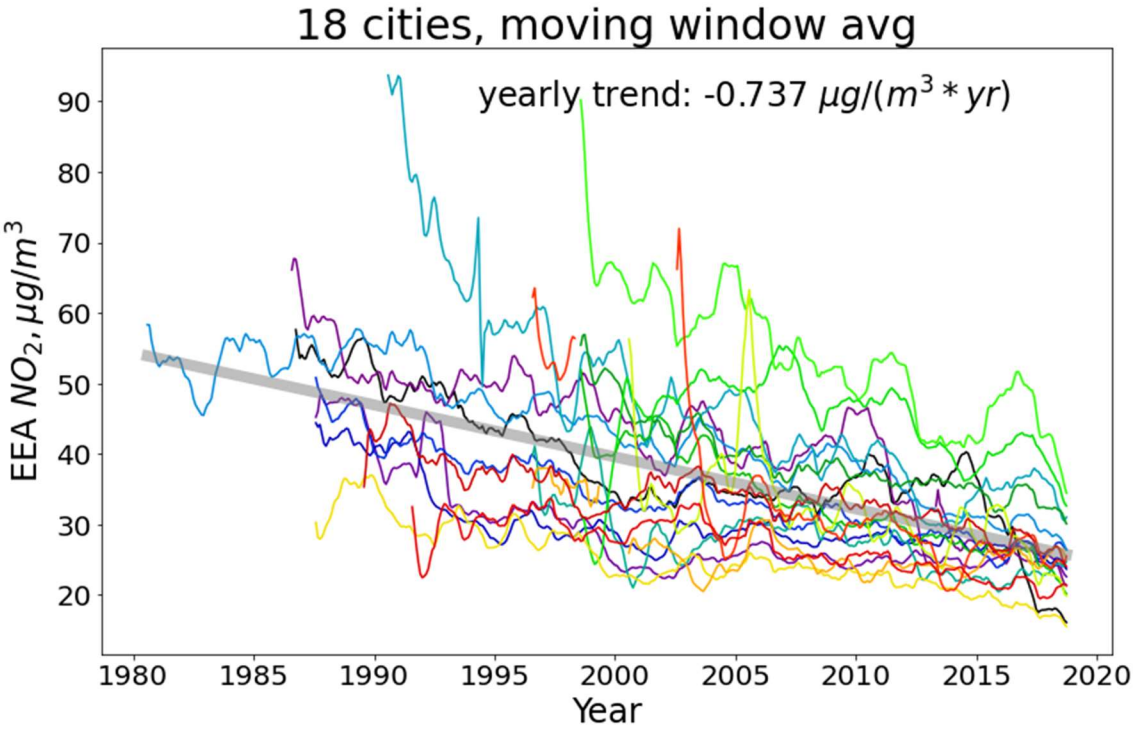

Figure 4-2 The NO_2 trend across the 18 European cities show an overall decreasing trend.

4.3. 5-year mean of diurnal cycle

The 5-year mean of hourly data help reveal whether the peaks and troughs of the NO_2 diurnal cycle have shifted in time and in amplitude (Figure 4-3).

Similar to the long-term trends, the mean NO_2 level decreased over time. In the 5-year means, the NO_2 levels in Bologna (Italy) and Prague (Czech Republic) are constantly lower than the 40 $\mu g/m^3$ limit.

All cites show two NO_2 peaks in one diurnal cycle, one in the morning and one in the evening. The peak in the morning can be explained by the low planetary boundary layer (PBL), the photolysis of NO_x reservoir species, and the morning rush hours; the peak in the evening can be attributed to the shrinking PBL, the conversion of NO_x to reservoir species, and the evening rush hours.

Many cities show observable changes in the timing of the peaks. Cities showing increasingly early morning peaks are: Dusseldorf (Germany), Rome and Milan (Italy), Vienna, Austria. The time of the evening peak, in comparison, does not seem to change significantly. On the other hand, the morning peaks in Lisbon (Portugal) and Brussels (Belgium) are arriving later through time.

The evening peak in Rome and Milan, Italy is arriving earlier in recent years, but the same trend was not observed in other cities.

One interesting observation is that the peak in the morning for many cities started to arrive earlier and earlier before 2005–2010, but became late after that. Such cities are: Birmingham (UK), Paris and Lyon (France), Prague (Czech Republic) and Brussels (Belgium). The evening peaks in those cities seem to have the same pattern, but it is not so

clear. For example, the evening peak in Paris, France in 2015–2020 arrives later than that in 2005–2010.

Glasgow (UK) and Madrid (Spain) show special diurnal patterns. Glasgow, UK is the only city where the evening peak arrived before 18:00. It is more like an "afternoon peak" in Glasgow, UK, and the interval between two peaks is significantly shorter than that in other cities. In Madrid, the mean NO_2 diurnal cycle before 2000 showed little to no decrease in the afternoon, and one may reach the conclusion that there is only one NO_2 peak during the day before 2000.

4.4. Trend of each hour

This section investigates whether the decrease in NO_2 is more significant at 12 pm over the years, compared to 5 pm.

Comparing the trend of different hours or periods (e.g. 9 am–12 pm vs 3 pm–6 pm) may reveal different trends at different hours.

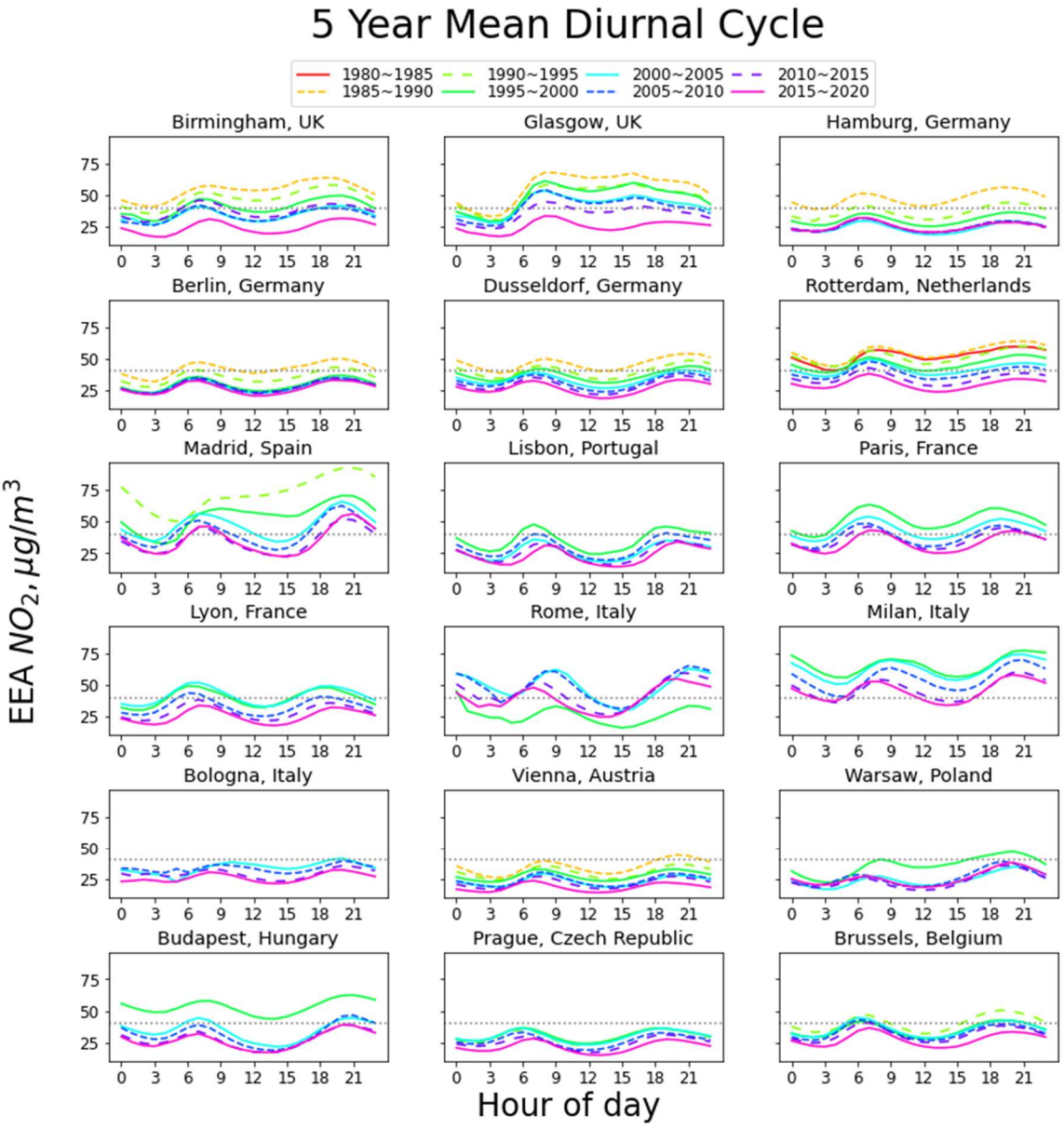

Figure 4-3 The 5-year mean diurnal cycle in EEA data shows that some of the cities have experienced change in the diurnal cycle over the years.

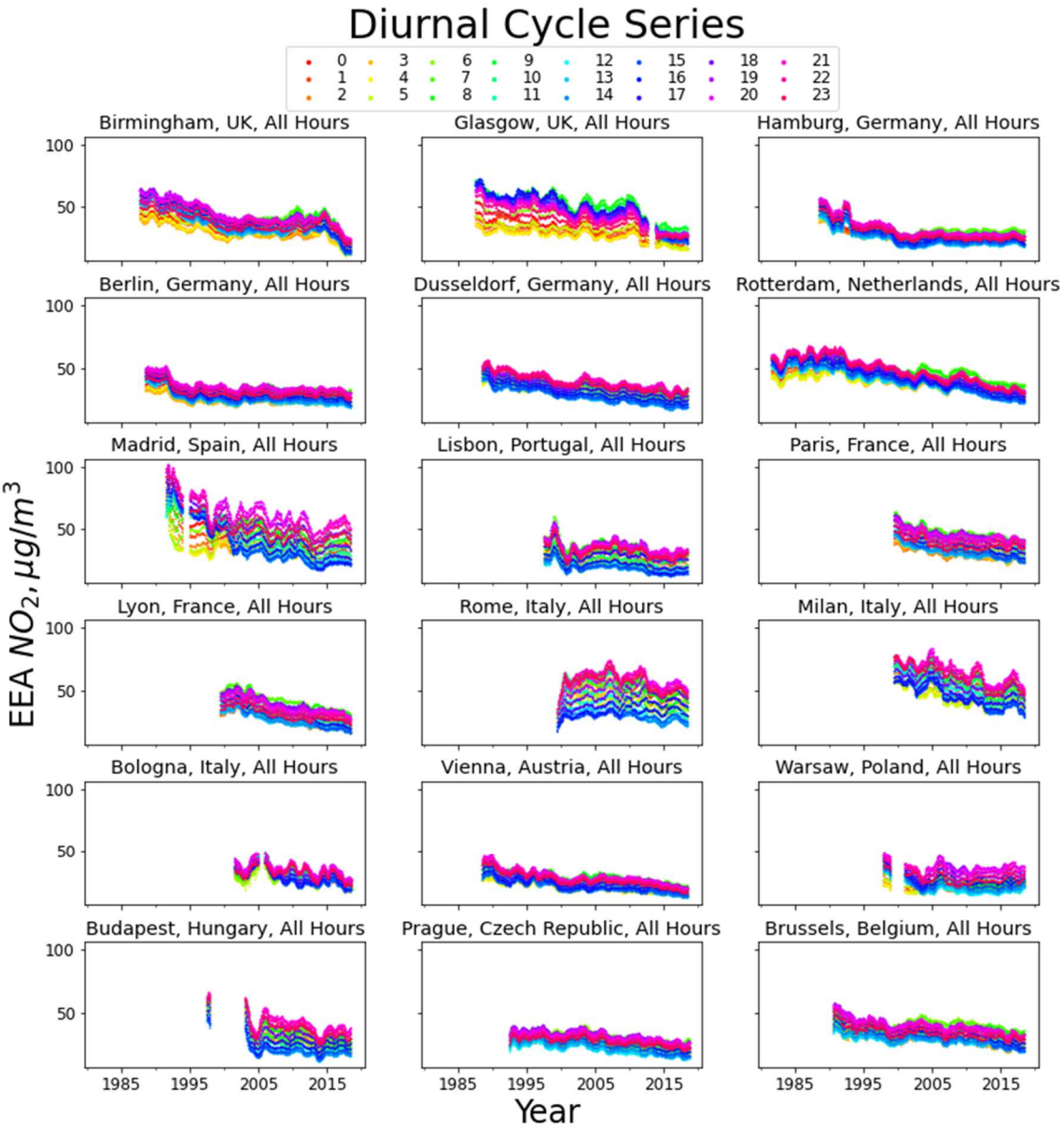

Figure 4-4 Monthly mean NO_2 time series of each hour of the day without the seasonal component shows that the relative level of morning and afternoon NO_2 have changed over time in some cities.

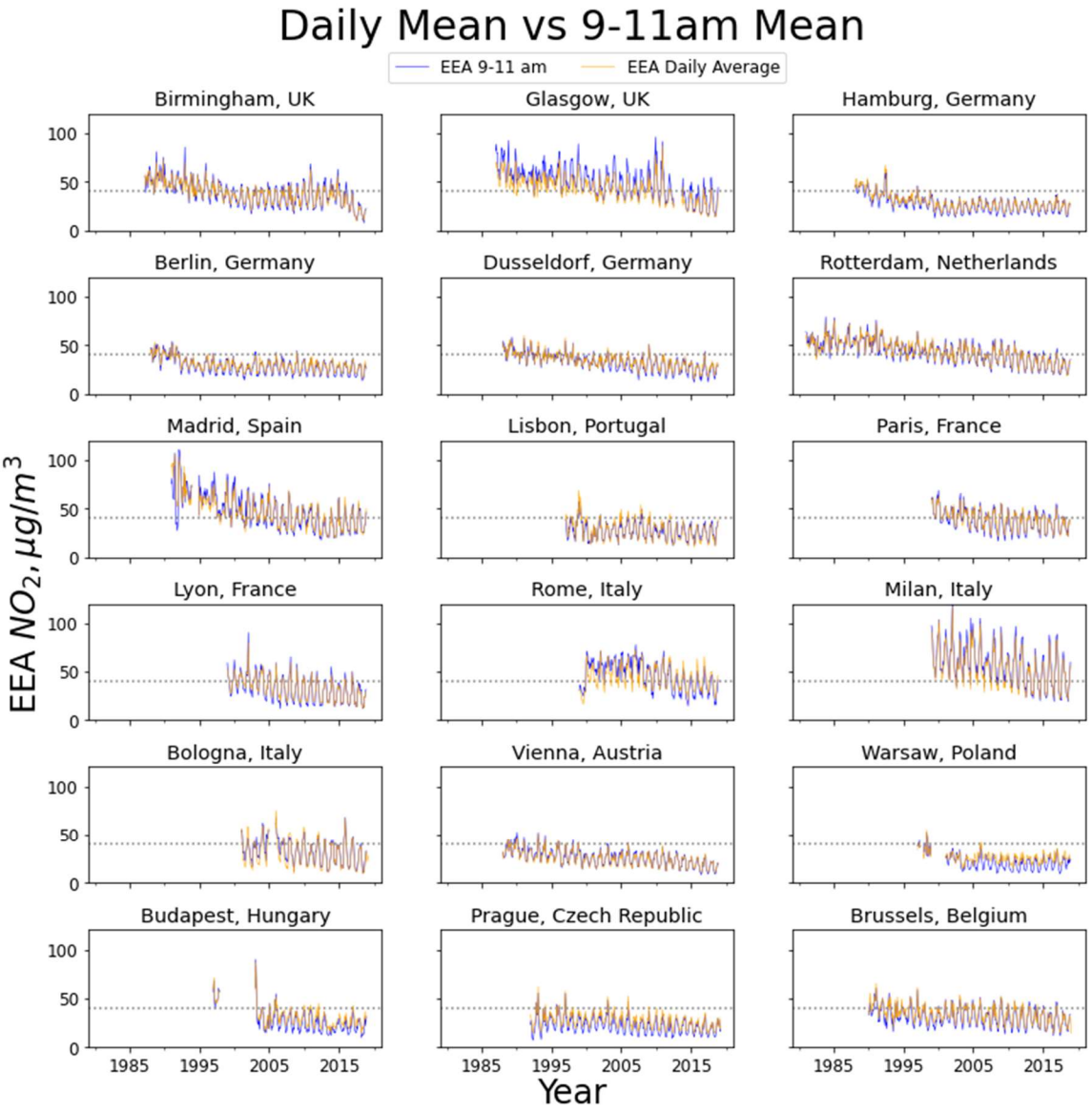

Figure 4-5 In the long run, the daily mean NO_2 and 9-11am mean NO_2 are quite similar.

By removing the seasonality in the time series of each hour of day, the underlying trend becomes more obvious (Figure 4-4). For example, starting in the early 2000s, the morning NO_2 in Glasgow (UK) and Rotterdam (Netherlands) stands out compared to the afternoon NO_2. The morning NO_2 in Birmingham (UK) and Madrid (Spain) is below the afternoon NO_2 hours in the 1990s, but became higher in the 2000s.

However, if we compare the time series of daily mean NO_2 with the mean NO_2 between 9 am–11 am local time, the two series are very similar (Figure 4-5). In the following studies, the 9 am–11 am local time mean NO_2 is used.

4.5. 5-year mean of seasonal cycle

In different seasons, NO_2 emission from human activity may change, such as the need to commute or the need for heating; the dispersion of NO_2 near the surface is affected by changes in the PBL height and the wind pattern. Taking 5-year averages of the daily mean NO_2 of each month of the year helps to reveal whether the intra-annual cycles in different cities have changed over time.

Figure 4-6 shows the change in 5-year mean seasonal cycles of the 18 cities selected. All of them have a dip in the middle of the calendar year, which can be attributed to the expansion of PBL in the Northern Hemisphere and increase in wind speed in the boreal summer.

After 2000, the peaks in all selected cities are in December to February, except those in the UK. Before the 2000s, we observed peaks in March–June in the UK and Germany and a sudden rise of NO_2 in May and June in Warsaw, Poland, in 1995–2000.

Some other interesting observations are the universal peak in November across the UK in the late 1980s, the weak NO_2 seasonality in the UK and Germany, the sudden decrease in NO_2 levels across Germany in the early 1990s, the persistent low in Milan and Rome, Italy in August and the significant peaks in Budapest, Hungary in 1995–2005 which

disappeared afterwards. There is also a peak in March in Paris, France, which also disappeared after 2005.

Some cities show strange NO_2 seasonality in their early NO_2 records: Madrid (Spain) shows low seasonality and high NO_2 level throughout the year; Warsaw (Poland) shows peaks in 1995–2000 April and September which was not observed afterwards.

4.6. Trend Reversal

Some EEA records have a gap in the middle of the time series, sometimes longer than a year. Those records were divided into sections, and trend reversal detection is run on each section to find possible reversals.

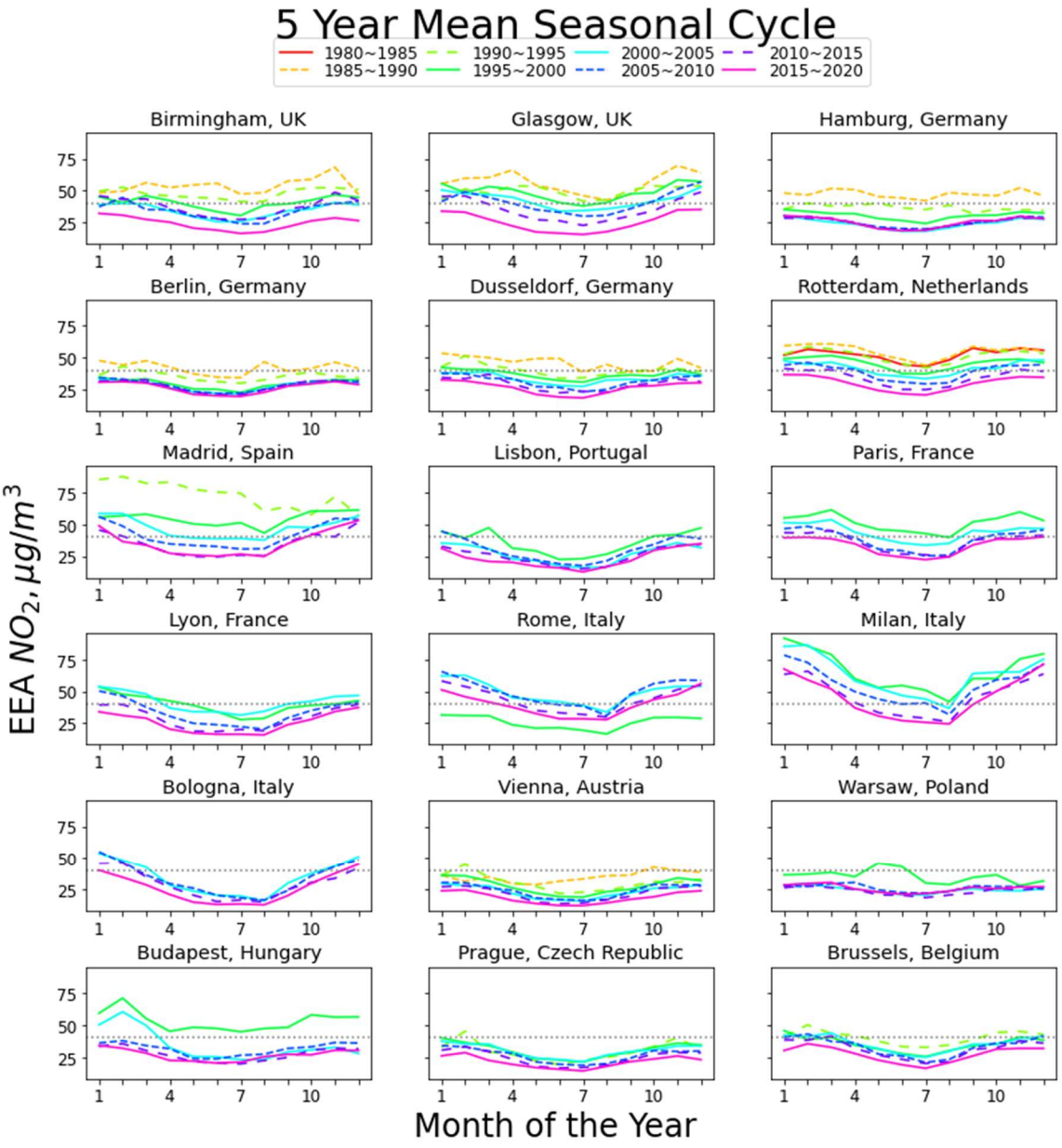

Figure 4-6 The 5-year mean seasonal cycle of the EEA data in the selected cities. The seasonal cycle in most cities is stable since the 2000s.

Using the trend reversal detection algorithm described in chapter 3, trend reversals were found in most of the 18 European cities selected. However, the timing of the trend reversal in EEA NO_2 time series are different from those in the satellite-derived

tropospheric column density, leading to the question whether the trend reversals in the satellite data are robust. In fact, among the 18 cities selected for analysis, the only 4 cities showing agreement of trend reversal between ground station measurements (EEA data) and satellite-derived NO_2 are: Hamburg (Germany), Vienna (Austria), Warsaw (Poland) and Budapest (Hungary). Based on the satellite data, trend changes in the early 2000s are common across the EU, and one can see similar phenomena in Figure 4-5, but the trend reversal detection results disagree (Figure 4-7). In some of the cities, such as Madrid (Spain), Lisbon (Portugal) and Paris (France), trend reversals detected in ground stations and satellite NO_2 are in the same year, but the trend reversals are different. For the three cities, NO_2 trends in the satellite time series are from positive to negative, while in the ground station measurements, the NO_2 trends are from negative to positive, even though their long-term NO_2 levels are decreasing.

There are some cases where trend reversal is only detected in either the ground station data or the satellite data. For instance, there is a positive-to-negative trend change in Bologna, Italy according to the satellite-derived NO_2 column in the early 2000s, but no significant trend change was detected in the EEA's NO_2 time series. Another example is a positive-to-negative trend reversal detected in Rome, Italy in around 2004. The trend change was detected in the EEA data, but no trend change could be detected in the satellite data. Even though some trend reversals can be detected in the overlapping observation period, the point where they happen may differ. The trend reversal point in Birmingham, UK was detected in the early 2000s in the satellite data, but the reversal point was about a decade late in the EEA data.

To gain more insight about the trend change detection, let's focus on one city. For example, a maximum trend reversal has been detected in the EEA NO_2 in Glasgow (UK) between 1990–1995 while a trend reversal has been detected in satellite time series around 2004. If we restrict the detection only to data after 1996, then we obtain a maximum trend reversal 2005, which seems to agree well with the satellite time series. However, because the trend reversal detection algorithm is designed to pick only one change point in the whole time series, our result indicates that there may be more than one trend change points in the NO_2 time series but they have been ignored in the detection. More importantly, "trend changes" is probably a misnomer; instead, what has been known as "trend change points" might be turning points of a periodic signal. Because we have been using 5-year left and right windows when searching for the trend change points, the periodic signal being detected may actually correspond to a decadal process of period of about 10 years. We found similar conclusions for Berlin, Dusseldorf (Germany) and Rotterdam (Netherlands), where we identified trend change points outside the period examined by Georgoulias et al.

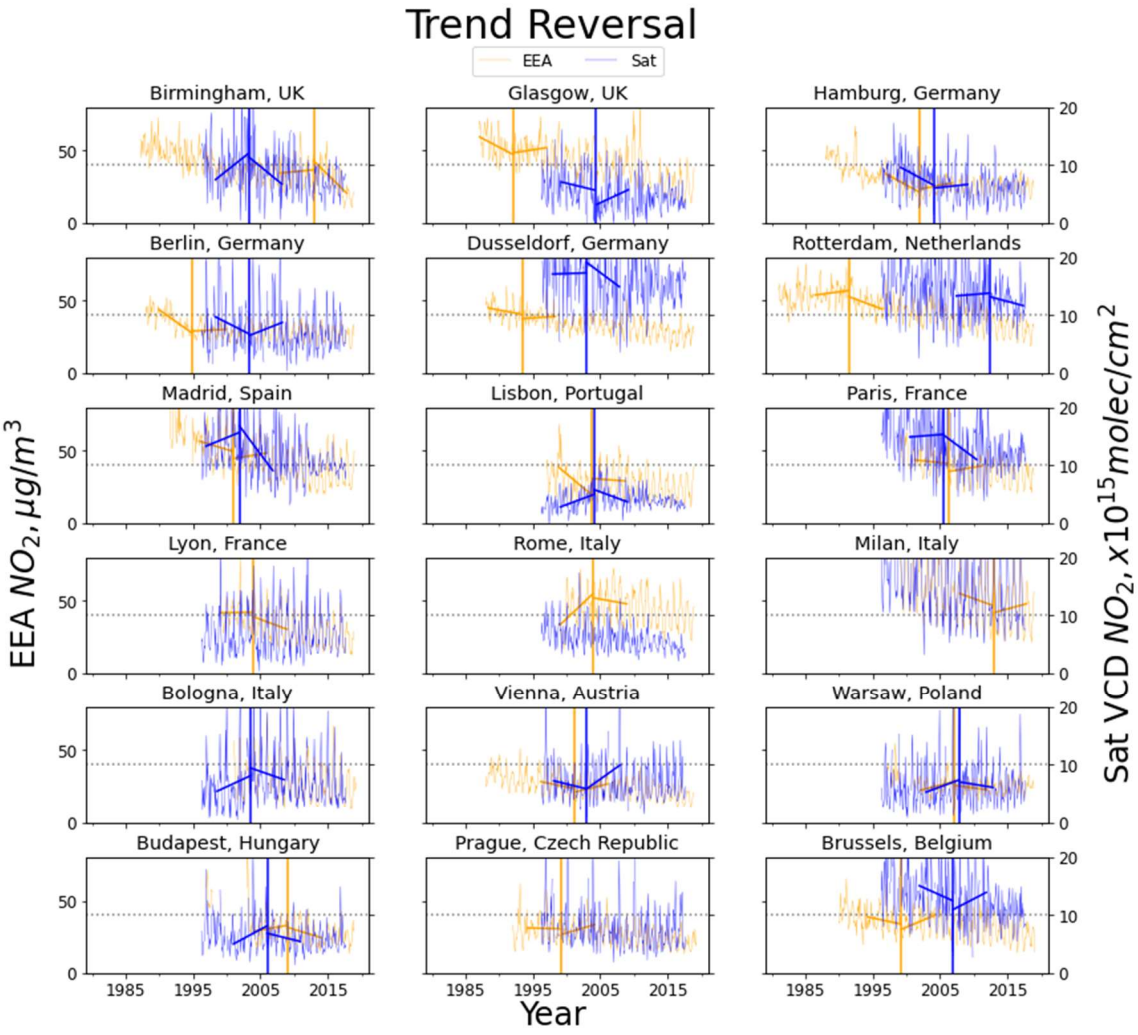

Figure 4-7 Trend reversal point and trend line before and after the reversal in EEA and satellite data. No trend reversals in the satellite data were detected in Lyon (France), Rome (Italy) and Milan (Italy).

5 Discussion

5.1. Conclusion

While a major disadvantage of air quality networks at the surface is their sparse distribution and low spatial coverage, their high temporal coverage, both in length and frequency, offer an opportunity for a definitive study of the NO_2 trends in different times of the day, assuming the biases in chemiluminescence NO_x analyzers using catalytic converters do not vary on a decadal time scale. In this study, NO_2 data from two EEA datasets were combined and compared with reanalysis and satellite data. The EEA data presented more consistent seasonality, compared to the satellite data where the outliers and noise caused weak and unrealistic seasonal cycles.

Another advantage of EEA data is the distinction between background and traffic stations, as well as urban and rural area types. EPA only has location setting (urban, suburban, rural) and land use (residential, agricultural, commercial…) therefore we did not analyze the EPA data even though county-wise and station-wise monthly averaged time series datasets have been compiled from raw EPA data.

The EEA data in 18 European cities have all shown long-term reduction in the NO_2 concentrations over urban-background sites. The increased NO_2 concentrations over some ground stations in Germany may be explained by increased traffic due to urbanization and urban development, offsetting the potential effects of the implementation of emission reduction efforts. In addition, several cities, such as Rome, Italy, have not met the long-

term NO_2 standard, highlighting the need for further regulations in order to minimize the health effect of NO_2 on human health.

The trend changes detected in the EEA data partially agree with the findings by Georgoulias et al. (2019), where most positive-to-negative trend reversals in the EU were found to be in the early 2000s. With longer NO_2 record from the EEA database, we showed evidence that the trend change detection algorithm may have detected decadal variability in the NO_2 time series rather than changes in the trend. The cause of the decadal variability warrants further investigation.

In the European open power plants database created by Joint Research Centre (JRC) in European Commission, 134 fossil fuel power plants were commissioned in 2000–2005, while 121 were commissioned in 1990–1999 and only 58 were commissioned in 1990–1995. Only 102 fossil fuel power plants were recorded to be decommissioned, and the first one on record was in 2007. The sudden increase in the number of power plants may be a reason why the NO_2 level rose in the early 2000s in Europe. The introduction of EURO 3 standard in 2001 which first set a limit on vehicle NO_x emission by itself, and EURO 4 standards where the limit became about 53% of that of EURO 3. They may have played a role in the change of trend to a decreasing trend in the EU after the early 2000s. The 11-year solar cycle may also have an impact on the rise in the surface level concentration of NO_2 through O_3 photolysis but this effect is not studied in this thesis.

There are also difficulties explaining some trend reversals detected in the EEA time series. The financial crisis in 2008 should have an impact on the NO_2 trend as well, but its effect on the NO_2 trend is only detected in Budapest, Hungary. The trend reversals in the

1990s were also hard to explain, compared to the reversals detected in the 2000s in the same city using the satellite data. In the meanwhile, there are also some cases where the trend reversal is found only in the EEA or the satellite time series.

5.2. Systematic error

Ground stations may overestimate the NO_2 concentration (Matthews et al., 1977; Ordóñez et al., 2006; Steinbacher et al., 2007; Winer et al., 1974). Some studies have tried to correct for the bias in MoO_x converters and get better NO_2 concentration data (Lamsal et al., 2008, 2010, 2013, 2014), but we didn't attempt it based on the following reasons:

1. Differences between MoO_x readings and Photolytic readings are site-specific, and depend on local NO_z, local meteorological conditions, site-source distance (photochemical aging), individual monitor calibration, etc. Therefore the correction factor from one MoO_x + Photolytic AQS (e.g. 1.2) cannot be applied to other MoO_x-only sites (Lamsal et al., 2015).
2. We are looking at the long-term trend. The effects of NO_z on MoO_x converters should not affect the long-term trend and change in trend.
3. In highly polluted areas, NO_x is more dominant in NO_y; at remote sites (less polluted areas), we expect to see more NO_z effects. We are looking at large cities, and the NO_z effects should be minimized. Also, when taking the station readings in an area, the spatial heterogeneity in ground NO_2 measurements will have reduced effect and the trend should be robust (Lamsal et al., 2015).

5.3. The disadvantages of the trend reversal detection algorithm

Our trend reversal detection shows that 10 out of 18 cities are showing negative-to-positive trend reversals. That is more than half of the cities we selected for analysis but is not consistent with the overall decreasing trend of NO_2 in those cities.

This is likely caused by the trend reversal detection algorithm itself, which only detect the most significant trend reversal. If there are more than one trend reversals in the time series, the trend reversal detection algorithm will not be able to capture them all; the positive-to-negative trend reversals may not be detected if the trends before and after are not statistically significant. For instance, the negative-positive-negative trend in Birmingham, UK is obvious on Figure 4-5, where the negative-to-positive trend reversal happened in early 2000s and the positive-to-negative trend reversal happened in around 2012. The trend reversal detection algorithm only captured the latter.

The continuous change detection and classification algorithm (Zhu and Woodcock, 2014) may be useful in detecting multiple trend reversals in a time series, but it will not be so comparable with the satellite time series since it's a different algorithm. Also, in the continuous change detection and classification algorithm, the 3σ limit for a trend change is an empirical standard, which is unlikely suitable for the NO_2 time series.

Another possible way to improve the trend change detection algorithm is to use the troughs in the S(t) values and detect the corresponding trend significance before and after the possible trend reversal point(s). In practice, the S(t) values turned out to be too noisy for continuous trough detection, and an empirical limit may need to be applied to filter out

the spikes. In conclusion, the lack of ability to detect multiple trend reversals is an issue that needs to be addressed in further studies.

van der A., R. J., Eskes, H. J., Boersma, K. F., van Noije, T. P. C., Van Roozendael, M., De Smedt, I., Peters, D. H. M. U. and Meijer, E. W.: Trends, seasonal variability and dominant NOx source derived from a ten year record of NO2 measured from space, J. Geophys. Res. Atmos., 113(4), 1–12, doi:10.1029/2007JD009021, 2008.

Behrens, L. K., Hilboll, A., Richter, A., Peters, E., Eskes, H. and Burrows, J. P.: GOME-2A retrievals of tropospheric NO2 in different spectral ranges-influence of penetration depth, Atmos. Meas. Tech., 11(5), 2769–2795, doi:10.5194/amt-11-2769-2018, 2018.

Boersma, K. F., Jacob, D. J., Eskes, H. J., Pinder, R. W., Wang, J. and van der A, R. J.: Intercomparison of SCIAMACHY and OMI tropospheric NO2 columns: Observing the diurnal evolution of chemistry and emissions from space, J. Geophys. Res. Atmos., 113(16), 1–14, doi:10.1029/2007JD008816, 2008.

Cermak, J., Wild, M., Knutti, R., Mishchenko, M. I. and Heidinger, A. K.: Consistency of global satellite-derived aerosol and cloud data sets with recent brightening observations, Geophys. Res. Lett., 37(21), 1–5, doi:10.1029/2010GL044632, 2010.

Chen, J., de Hoogh, K., Gulliver, J., Hoffmann, B., Hertel, O., Ketzel, M., Bauwelinck, M., van Donkelaar, A., Hvidtfeldt, U. A., Katsouyanni, K., Janssen, N. A. H., Martin, R. V., Samoli, E., Schwartz, P. E., Stafoggia, M., Bellander, T., Strak, M., Wolf, K., Vienneau, D., Vermeulen, R., Brunekreef, B. and Hoek, G.: A comparison of linear regression, regularization, and machine learning algorithms to develop Europe-wide spatial models of fine particles and nitrogen dioxide, Environ. Int., 130(June), doi:10.1016/j.envint.2019.104934, 2019.

Dignon, J.: NOx and SOx emissions from fossil fuels: A global distribution, Atmos. Environ. Part A, Gen. Top., 26(6), 1157–1163, doi:10.1016/0960-1686(92)90047-O, 1992.

Dunlea, E. J., Herndon, S. C., Nelson, D. D., Volkamer, R. M., San Martini, F., Sheehy, P. M., Zahniser, M. S., Shorter, J. H., Wormhoudt, J. C., Lamb, B. K., Allwine, E. J., Gaffney, J. S., Marley, N. A., Grutter, M., Marquez, C., Blanco, S., Cardenas, B., Retama, A., Yillegas, C. R. R., Kolb, C. E., Molina, L. T. and Molina, M. J.: Evaluation of nitrogen dioxide chemiluminescence monitors in a polluted urban environment, Atmos. Chem. Phys., 7(10), 2691–2704, doi:10.5194/acp-7-2691-2007, 2007.

Gardner, R. M., Adams, K., Cook, T., Deidewig, F., Ernedal, S., Falk, R., Fleuti, E., Herms, E., Johnson, C. E., Lecht, M., Lee, D. S., Leech, M., Lister, D., Massé, B., Metcalfe, M., Newton, P., Schmitt, A., Vandenbergh, C. and Van Drimmelen, R.: The ANCAT/EC global inventory of NO(x) emissions from aircraft, Atmos. Environ., 31(12), 1751–1766, doi:10.1016/S1352-2310(96)00328-7, 1997.

Geddes, J. A., Martin, R. V., Boys, B. L. and van Donkelaar, A.: Long-term trends worldwide in ambient NO2 concentrations inferred from satellite observations, Environ. Health Perspect., 124(3), 281–289, doi:10.1289/ehp.1409567, 2016.

Georgoulias, A. K., Van Der, R. A. J., Stammes, P., Folkert Boersma, K. and Eskes, H. J.: Trends and trend reversal detection in 2 decades of tropospheric NO2 satellite observations, Atmos. Chem. Phys., 19(9), 6269–6294, doi:10.5194/acp-19-6269-2019, 2019.

Gualtieri, G., Crisci, A., Tartaglia, M., Toscano, P., Vagnoli, C., Andreini, B. P. and Gioli, B.: Analysis of 20-year air quality trends and relationship with emission data: The case of Florence (Italy), Urban Clim., 10(P3), 530–549, doi:10.1016/j.uclim.2014.03.010, 2014.

Guerreiro, C. B. B., Foltescu, V. and de Leeuw, F.: Air quality status and trends in Europe, Atmos. Environ., 98, 376–384, doi:10.1016/j.atmosenv.2014.09.017, 2014.

Haagen-Smit, A.: The Air Pollution Problem in Los Angeles, Eng. Sci., 14(3), 7–13, 1950.

Haagen-Smit, A. J.: Chemistry and Physiology of Los Angeles Smog, Ind. Eng. Chem., 44(6), 1342–1346, doi:10.1021/ie50510a045, 1952.

Henschel, S., Querol, X., Atkinson, R., Pandolfi, M., Zeka, A., Le Tertre, A., Analitis, A., Katsouyanni, K., Chanel, O., Pascal, M., Bouland, C., Haluza, D., Medina, S. and Goodman, P. G.: Ambient air SO2 patterns in 6 European cities, Atmos. Environ., 79, 236–247, doi:10.1016/j.atmosenv.2013.06.008, 2013.

Henschel, S., Le Tertre, A., Atkinson, R. W., Querol, X., Pandolfi, M., Zeka, A., Haluza, D., Analitis, A., Katsouyanni, K., Bouland, C., Pascal, M., Medina, S. and Goodman, P. G.: Trends of nitrogen oxides in ambient air in nine European cities between 1999 and 2010, Atmos. Environ., 117, 234–241, doi:10.1016/j.atmosenv.2015.07.013, 2016.

Jacob, D. J.: Introduction to Atmospheric Chemistry, Exopl. Atmos., 92–109, doi:10.2307/j.ctvc77ddr.10, 2019.

Keuken, M., Roemer, M. and van den Elshout, S.: Trend analysis of urban NO2 concentrations and the importance of direct NO2 emissions versus ozone/NOx equilibrium, Atmos. Environ., 43(31), 4780–4783, doi:10.1016/j.atmosenv.2008.07.043, 2009.

Kim, S. W., Heckel, A., McKeen, S. A., Frost, G. J., Hsie, E. Y., Trainer, M. K., Richter, A., Burrows, J. P., Peckham, S. E. and Grell, G. A.: Satellite-observed U.S. power plant

NOx emission reductions and their impact on air quality, Geophys. Res. Lett., 33(22), 1–5, doi:10.1029/2006GL027749, 2006.

Kim, S. W., Heckel, A., Frost, G. J., Richter, A., Gleason, J., Burrows, J. P., McKeen, S., Hsie, E. Y., Granier, C. and Trainer, M.: NO2 columns in the western United States observed from space and simulated by a regional chemistry model and their implications for NO x emissions, J. Geophys. Res. Atmos., 114(11), 1–29, doi:10.1029/2008JD011343, 2009.

Konovalov, I. B., Beekmann, M., Richter, A., Burrows, J. P. and Hilboll, A.: Multi-annual changes of NOx emissions in megacity regions: Nonlinear trend analysis of satellite measurement based estimates, Atmos. Chem. Phys., 10(17), 8481–8498, doi:10.5194/acp-10-8481-2010, 2010.

Lamsal, L. N., Martin, R. V., van Donkelaar, A., Steinbacher, M., Celarier, E. A., Bucsela, E., Dunlea, E. J. and Pinto, J. P.: Ground-level nitrogen dioxide concentrations inferred from the satellite-borne Ozone Monitoring Instrument, J. Geophys. Res. Atmos., 113(16), 1–15, doi:10.1029/2007JD009235, 2008.

Lamsal, L. N., Martin, R. V., Van Donkelaar, A., Celarier, E. A., Bucsela, E. J., Boersma, K. F., Dirksen, R., Luo, C. and Wang, Y.: Indirect validation of tropospheric nitrogen dioxide retrieved from the OMI satellite instrument: Insight into the seasonal variation of nitrogen oxides at northern midlatitudes, J. Geophys. Res. Atmos., 115(5), 1–15, doi:10.1029/2009JD013351, 2010.

Lamsal, L. N., Martin, R. V., Parrish, D. D. and Krotkov, N. A.: Scaling relationship for NO2 pollution and urban population size: A satellite perspective, Environ. Sci. Technol., 47(14), 7855–7861, doi:10.1021/es400744g, 2013.

Lamsal, L. N., Krotkov, N. A., Celarier, E. A., Swartz, W. H., Pickering, K. E., Bucsela, E. J., Gleason, J. F., Martin, R. V., Philip, S., Irie, H., Cede, A., Herman, J., Weinheimer, A., Szykman, J. J. and Knepp, T. N.: Evaluation of OMI operational standard NO2 column retrievals using in situ and surface-based NO2 observations, Atmos. Chem. Phys., 14(21), 11587–11609, doi:10.5194/acp-14-11587-2014, 2014.

Lamsal, L. N., Duncan, B. N., Yoshida, Y., Krotkov, N. A., Pickering, K. E., Streets, D. G. and Lu, Z.: U.S. NO2 trends (2005-2013): EPA Air Quality System (AQS) data versus improved observations from the Ozone Monitoring Instrument (OMI), Atmos. Environ., 110(2), 130–143, doi:10.1016/j.atmosenv.2015.03.055, 2015.

Mangia, C., Bruni, A., Cervino, M. and Gianicolo, E. A. L.: Sixteen-year air quality data analysis of a high environmental risk area in Southern Italy, Environ. Monit. Assess., 183(1–4), 555–570, doi:10.1007/s10661-011-1940-y, 2011.

Matthews, R. D., Sawyer, R. F. and Schefer, R. W.: Interferences in Chemiluminescent Measurement of NO and NO2 Emissions from Combustion Systems, Environ. Sci. Technol., 11(12), 1092–1096, doi:10.1021/es60135a005, 1977.

Mauzerall, D. L., Sultan, B., Kim, N. and Bradford, D. F.: NOx emissions from large point sources: Variability in ozone production, resulting health damages and economic costs, Atmos. Environ., 39(16), 2851–2866, doi:10.1016/j.atmosenv.2004.12.041, 2005.

McDonald, B. C., Dallmann, T. R., Martin, E. W. and Harley, R. A.: Long-term trends in nitrogen oxide emissions from motor vehicles at national, state, and air basin scales, J. Geophys. Res. Atmos., 117(17), 1–11, doi:10.1029/2012JD018304, 2012.

Munro, R., Lang, R., Klaes, D., Poli, G., Retscher, C., Lindstrot, R., Huckle, R., Lacan, A., Grzegorski, M., Holdak, A., Kokhanovsky, A., Livschitz, J. and Eisinger, M.: The GOME-2 instrument on the Metop series of satellites: Instrument design, calibration, and level 1 data processing - An overview, Atmos. Meas. Tech., 9(3), 1279–1301, doi:10.5194/amt-9-1279-2016, 2016.

Ordóñez, C., Richter, A., Steinbacher, M., Zellweger, C., Nüß, H., Burrows, J. P. and Prévôt, A. S. H.: Comparison of 7 years of satellite-borne and ground-based tropospheric NO2 measurements around Milan, Italy, J. Geophys. Res. Atmos., 111(5), 1–12, doi:10.1029/2005JD006305, 2006.

Richter, A., Eyring, V., Burrows, J. P., Bovensmann, H., Lauer, A., Sierk, B. and Crutzen, P. J.: Satellite measurements of NO2 from international shipping emissions, Geophys. Res. Lett., 31(23), 1–4, doi:10.1029/2004GL020822, 2004.

Russell, A. R., Valin, L. C., Bucsela, E. J., Wenig, M. O. and Cohen, R. C.: Space-based constraints on spatial and temporal patterns of NOx emissions in California, 2005-2008, Environ. Sci. Technol., 44(9), 3608–3615, doi:10.1021/es903451j, 2010.

Stavrakou, T., Müller, J. F., Boersma, K. F., De Smedt, I. and van der A, R. J.: Assessing the distribution and growth rates of NOx emission sources by inverting a 10-year record of NO2 satellite columns, Geophys. Res. Lett., 35(10), 1–5, doi:10.1029/2008GL033521, 2008.

Steinbacher, M., Zellweger, C., Schwarzenbach, B., Bugmann, S., Buchmann, B., Ordóñez, C., Prevot, A. S. H. and Hueglin, C.: Nitrogen oxide measurements at rural sites in Switzerland: Bias of conventional measurement techniques, J. Geophys. Res. Atmos., 112(11), 1–13, doi:10.1029/2006JD007971, 2007.

U.S. EPA, L. U.-U. S. E. P. A.: Integrated science assessment for oxides of nitrogen (final report), Washingt. D.C. Contract No. EPA/600/R-08/071, doi:10.1080/00107510412331283531, 2016.

Winer, A. M., Peters, J. W., Smith, J. P. and Pitts, J. N.: Response of commercial chemiluminescent NO-NO2 analyzers to other nitrogen-containing compounds, Environ. Sci. Technol., 8(13), 1118–1121, doi:10.1021/es60098a004, 1974.

Xing, J., Pleim, J., Mathur, R., Pouliot, G., Hogrefe, C., Gan, C. M. and Wei, C.: Historical gaseous and primary aerosol emissions in the United States from 1990 to 2010, Atmos. Chem. Phys., 13(15), 7531–7549, doi:10.5194/acp-13-7531-2013, 2013.

Zhu, Z. and Woodcock, C. E.: Continuous change detection and classification of land cover using all available Landsat data, Remote Sens. Environ., 144, 152–171, doi:10.1016/j.rse.2014.01.011, 2014.

Appendix 1. EPA and EEA Data Description

1. Acquisition of EPA data

The EPA datasets used in this research are daily data and hourly data. They are pre-generated data files downloaded from the EPA Air Data website (https://aqs.epa.gov/aqsweb/airdata/download_files.html). The files in that website are updated twice per year. In each June, the data are updated to cover the prior year; in each December, the data are updated to include the Summer of that year.

Both daily and hourly data are Version 3.0.0 which was updated on December 01, 2015.

2. Fields of EPA data tables

Detailed description of each field in the data tables can be found in the following links:

https://aqs.epa.gov/aqsweb/airdata/FileFormats.html#_daily_summary_files

https://aqs.epa.gov/aqsweb/airdata/FileFormats.html#_hourly_data_files

Fields useful to this study:

Latitude: the monitoring site's angular distance north of the equator measured in decimal degrees.

Longitude: The monitoring site's angular distance east of the prime meridian measured in decimal degrees.

Datum: The Datum associated with the Latitude and Longitude measures. The datums for most stations are WGS84 and NAD83, and very few are NAD27. Stations with NAD27 datum does not have values for longitude and latitude, therefore are omitted when processing; after comparing the coordinates from NAD83 to WGS84, the difference between the geo-coordinates are negligible, therefore the difference were neglected when compiling the dataset.

Date Local: The calendar date of the sample in Local Standard Time at the monitor.

Time GMT: The time of day that sampling began on a 24-hour clock in Greenwich Mean Time. Using this field avoids dealing with different time zones in the US.

State Name: The name of the state where the monitoring site is located. “Canada” means the station is in Canada instead of the US. So is “Mexico”.

County Name: The name of the county where the monitoring site is located.

City Name: The name of the city where the monitoring site is located. This represents the legal incorporated boundaries of cities and not urban areas. For some of the stations, this field is “not a city”.

Sample Measurement: Only hourly data files have this field. The measured value in the standard units of measure for the parameter. In this study, the measured NO_2 level.

Arithmetic Mean: Only daily summary files have this field. The average (arithmetic mean) value of NO_2 for the day.

3. Acquisition of EEA data

The EEA datasets used in this research are hourly data.

The data collected before 2013-01-01 and that after 2013-01-01 are in different datasets.

Data before 2013-01-01 are AirBase v8 data, and it can be found in the following site, which has already expired:

https://www.eea.europa.eu/data-and-maps/data/airbase-the-european-air-quality-database-8

The page was archived on 25 Aug 2017, but the datasets from different EEA member states are still accessible, as well as the information of all stations.

The datasets before 2013-01-01 contain observations of different components (harmful substances), such as. CO, NO_2, SO_2, O_3 and PM_{10}. Each of the files in the dataset contains hourly observations of one component by one station, or summaries in one of the following ways: daily mean, 8-hourly mean, and daily max.

Information about stations and components measured comes with each EEA member country's data as a zip file. A table of all EEA stations can also be found in the same site.

Observations since 2013-01-01 come from two dataflows, namely E1a and E2a. E1a data are validated data reported by member states every September and cover data from the previous year; E2a are up-to-date hourly data which will be deleted when updating E1a data. In this study, since the E2a (unvalidated) dataset is small, both datasets are used.

URLs to data of both E1a and E2a can be found in the following site:

https://discomap.eea.europa.eu/map/fme/AirQualityExport.htm

Information about the stations can be directly downloaded from the above site which is updated on a daily basis.

4. Data format and contents

Product description of BEF2013 can be found in the same website as the download site.

The files containing observations are called “raw data files”. Those raw data files are tab-delimited text files and contain date and time (for hourly data) of observations as well as corresponding quality flags for each of them. For daily data, each row has data of all days in one calendar month; for hourly data, each row has data for all hours in one calendar day. Quality flags <=0 indicate invalid or missing data.

Many member countries in the EEA have their own naming conventions for the stations. In EEA, Exchange of Information (EoI) code is used to distinguish them. The file names of BEF2013 contain EoI code, pollutant code (00008 for NO_2), and data type (daily, daily maximum (“dymax”), 8-hourly and hourly).

For AFT2013, the columns useful to us are station local ID (“AirQualityStation”, “AirQualityStationEoICode”), station measurements (“Concentration”), measurement time (“DateTimeBegin”, “DateTimeEnd”) and quality flags (“Validity”, “Verification”). Longitude and Latitude of the stations can be retrieved from station information files using station local IDs. Most AFT2013 files only contain 1 station.

For EEA data, “Latitude” is the monitoring site’s angular distance north of the equator measured in decimal degrees, and “Longitude” is the monitoring site’s angular distance east of the prime meridian measured in decimal degrees. Stations to the west of the prime meridian have negative “Longitude” values.

For quality flags, “Validity” must equal to 1 to be valid and above instrument detection limit (http://dd.eionet.europa.eu/vocabulary/aq/observationvalidity/view); “Verification” must be equal to 1 to be “verified”. For the verification flag, 2 means “preliminary verified” and 3 means “not verified”.

Appendix 2. EEA Data Processing

1. BEF2013 processing

1.1. Read table, get the first 7 characters of the filename as the station ID.

1.2. Any measurement succeeded by a quality flag that is not 1 is replaced by NaN.

1.3. Drop quality flag columns, keep the date column.

1.4. Sort the table based on the date column, then get the start and end date of the observation.

1.5. From start date to end date, create date windows by the step of 1 month. For each date window, select all measurements within the date range, take the average along the date axis (i.e. the column; the hour axis is the row), therefore the monthly average.

1.6. Get the longitude and latitude from "bef2013_stations.csv", based on the station ID from the file name. Concatenate longitude and latitude to create "LonLat" and attach it to the table. "LonLat" column will be used as the station ID for merging.

1.7. Using the append method to attach all data tables to one csv file: hourly_sma.csv. SMA stands for "station monthly average".

2. AFT2013 processing

General processing is skipping France, Germany, Spain, and the UK, because those 4 countries use the "AirQualityStation" column instead of

“AirQualityStationEoICode”. Besides using the “AirQualityStation” column for station ID, the steps to process the data are the same.

General processing:

1. For each country and each station, read data table
2. Drop rows: Verification != 0 (keeping verified data), Validity<1 (keeping valid data), AveragingTime != “hour” (so it’s not daily measurements).
3. Based on unique stations of the table, iteratively select stations in the table (most tables only contain one station). Then, create variables: “date” based on the “DatetimeBegin” variable; “month” and “year”, from the “date” variable.
4. Use table1[‘Date’].dt.hour == hour to select a specific hour from the whole series, then table2.groupy(["year", "month"]) to group the subset based on year and month. Then use “aggregate” function to create the average for each year-month.
5. Create a “station” variable (column) based on the station selected; “hour” column based on the hour; “obs” column based on the number of observations in the year-month-hour. “Obs” variable has not proven to be useful yet.